Loading Induced Bone Adaptation in the Distal Radius of Women: Influence of Mechanical Environment

By

VARUN BHATIA
B.E., University of Mumbai, India, 2006
M.S., University of Illinois at Chicago, Chicago, 2009

THESIS
Submitted as partial fulfillment of the requirements
for the degree of Doctor of Philosophy in Bioengineering
in the Graduate College of the
University of Illinois at Chicago, 2013

Chicago, Illinois

Defense Committee:

Karen Troy, Chair and Advisor
D. Rick Sumner, Rush University
W. Brent Edwards, Kinesiology and Nutrition
Hannah Lundberg, Rush University
James Patton
Thomas Royston

Table of Contents

List of Tables

List of Figures

Summary

Bone adapts to the mechanical loads it experiences. This adaptive response takes place by bone modeling and remodeling, and is driven by the mechanical stimuli experienced by the bone. The degree to which bone adapts depends on the degree to which the mechanical stimulus deviates from some threshold stimulus values. This ability of bone to adapt to externally applied mechanical stimulus has allowed exercise-based interventions as a practical option to prevent bone loss and enhance bone strength. However, determining the mechanical stimulus thresholds required to initiate adaptive response is important to the success of such interventions.

The magnitude of the adaptive response has been attributed to the characteristics of the mechanical stimulus in animals. However, the contribution of the different mechanical stimulus characteristics to the adaptive process and the mechanical stimuli thresholds above which bone adaptation is initiated are currently unknown in humans. The objective of this research was to understand the quantitative relationship of human bone to its mechanical environment, with the long term goal of designing and evaluating exercise interventions to prevent or slow bone loss that can lead to osteoporosis, and improve fracture strength.

A novel *in-vivo* wrist loading model was used to accomplish the objectives of this research. Methods for subject specific finite element model generation to predict the surface strains at the distal radius were validated with high accuracy (r=0.968, RMSE=11.1%), and were used to assess loading-induced bone strain in the subjects. An increase (or the prevention of a decrease) in ultra-distal radius size and mass was the primary adaptation response to the axial compression of the radius, and this response was more directly related to strain magnitude than the force magnitude of the applied load. Additionally, small but significant correlations were

observed between changes in bone mineral density and the mechanical measures of the applied loads at the local level within the bone. Although a strain-dependant site-specific behavior has previously been shown in animals, to our knowledge, this was the first time that the localized adaptation behavior of bone was tested in humans.

In summary, we have developed an *in vivo* loading model of the human radius for the purpose of understanding influence of mechanical environment on bone adaptation. The loading task was capable of producing an osteogenic response, and along with the validated *in-vivo* FE model, we were able to test the relation between the mechanical characteristics of the applied loads and the resultant changes in the bone mineral parameters. In addition to its usefulness for exploring bone adaptation in humans, this research also acts as a step towards designing effective targeted mechanical interventions to increase (or prevent the decrease of) bone strength.

Chapter 1. Introduction

1.1 Background

Bone is a dynamic tissue that adapts its internal architecture and external conformation to the mechanical loads it experiences. This adaptive response takes place by bone modeling and remodeling, and is driven by the mechanical stimuli (strain, stress, strain energy density, etc.) experienced by the bone. The degree to which bone adapts depends on the degree to which the mechanical stimuli (sum of applied external stimuli and those applied by the activation of muscles) deviates from some threshold stimulus values (Figure 1-1). Net bone apposition occurs when the applied mechanical stimulus exceeds some maximum threshold, while net bone resorption occurs when the applied mechanical stimulus falls below a minimum threshold. Most activities however, result in a mechanical stimulus between the thresholds resulting in no net change, and the bone remains in a state of homeostasis.

Aging, menopause, and certain disorders have been associated with bone fragility and the increase in the occurrences of fractures. The ability of bone to adapt to mechanical stimuli has allowed exercise-based interventions as a practical option to prevent bone loss and enhance bone strength. However, determining the mechanical stimulus thresholds required to initiate adaptive response is important to the success of such interventions.

Several groups have attempted to describe the relationship between mechanical loading and bone adaptive response in both, animals and humans. In animals, the magnitude of the adaptive response has been attributed to the characteristics of the mechanical stimulus such as strain, strain rate, and number of loading cycles. These characteristics are assumed to regulate adaptation in humans as well, and exercise programs that incorporate these principles have been

tested with some success. Human bone likely behaves in a fundamentally similar manner to animal bones; however the details of the adaptive process may differ between species. The contribution of the different mechanical stimulus characteristics to the adaptive process, and the mechanical stimuli thresholds above which bone adaptation is initiated, is currently unknown in humans.

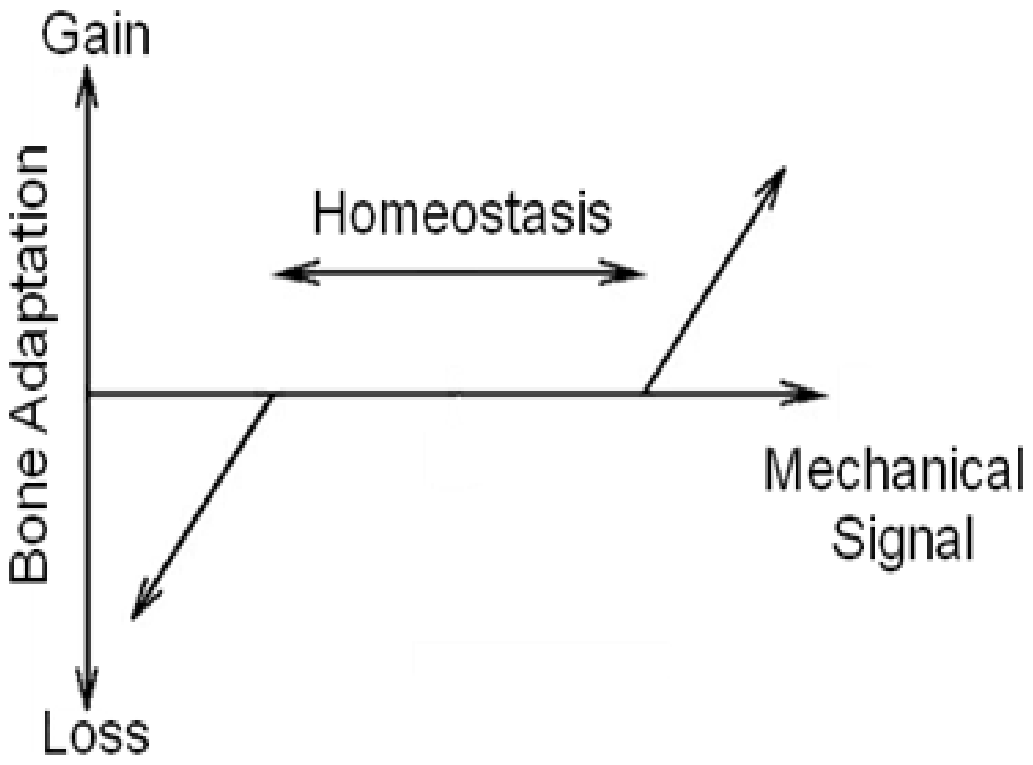

Figure 1-1: Adaptive response to applied stimuli. (Adapted from Carter DR, 1984)

The objective of this research is to understand the quantitative relationship of human bone to its mechanical environment, with the long term goal of designing and evaluating exercise interventions to a) prevent or slow bone loss that can lead to osteoporosis and increased fracture risks, b) increase peak bone mass, and/or bone structural properties earlier in life to improve fracture strength.

1.2 Experiment Design

To accomplish the above mentioned objective, three aims are proposed (Figure 1-2). For the first aim, finite element (FE) methods will be developed and validated using cadaveric specimens to predict strains experienced by the distal radius during the exercise task described below. The second aim will use image analyses and FE methods to determine whether the exercise task is osteogenic. The third aim will use the same tools to relate the local bone adaptation with the local mechanical environment. Both aim 2 and 3 will use an exercise regime involving healthy women assigned to either a control group or exercise group. The exercise groups will undergo a mechanical loading regimen that involves leaning onto the palm of the hand three days a week for six months, during which their distal radius properties and muscle volume will be non-invasively quantified. The women in the exercise group will be divided into two more groups, a fixed force group wherein all subjects will be assigned the same loading magnitude and a fixed strain group where each subject will be assigned a loading magnitude corresponding to the same strain magnitude.

Aim 1: Create methods for subject specific finite element models used to predict surface strains at the distal radius during an exercise task, and validate the methods with cadaveric testing.

Aim 2a: Determine whether the prescribed exercise regime is osteogenic by comparing whole bone BMC and fracture strength at baseline and after the exercise regime.

Hypothesis 2a: Increase in whole bone BMC and fracture strength will be observed as a result of exercise.

Aim 2b: If hypothesis 2a is supported, then determine whether change in BMC is more closely related to force magnitude or strain magnitude by comparing a fixed force exercise group to a fixed strain exercise group.

Hypothesis 2b: Changes will be more directly related to the strain magnitude than the load magnitude

Aim 3: Determine the degree to which local adaptation within a given bone depends on the local mechanical environment, by comparing local adaptation with the corresponding strains.

Hypothesis 3: Changes in the bone will be site specific and will be observed at locations experiencing strains above some threshold strain value. Above this threshold, changes will be proportional to the strain magnitude.

This research aims at translating relationships previously demonstrated in animal to humans, and is significant because it will improve the understanding of the relation between applied stimulus and bone adaptation response. Overall, the outcomes of this study will act as an important step in the development of methods to design and evaluate exercise interventions which will be used to improve bone health and prevent fractures.

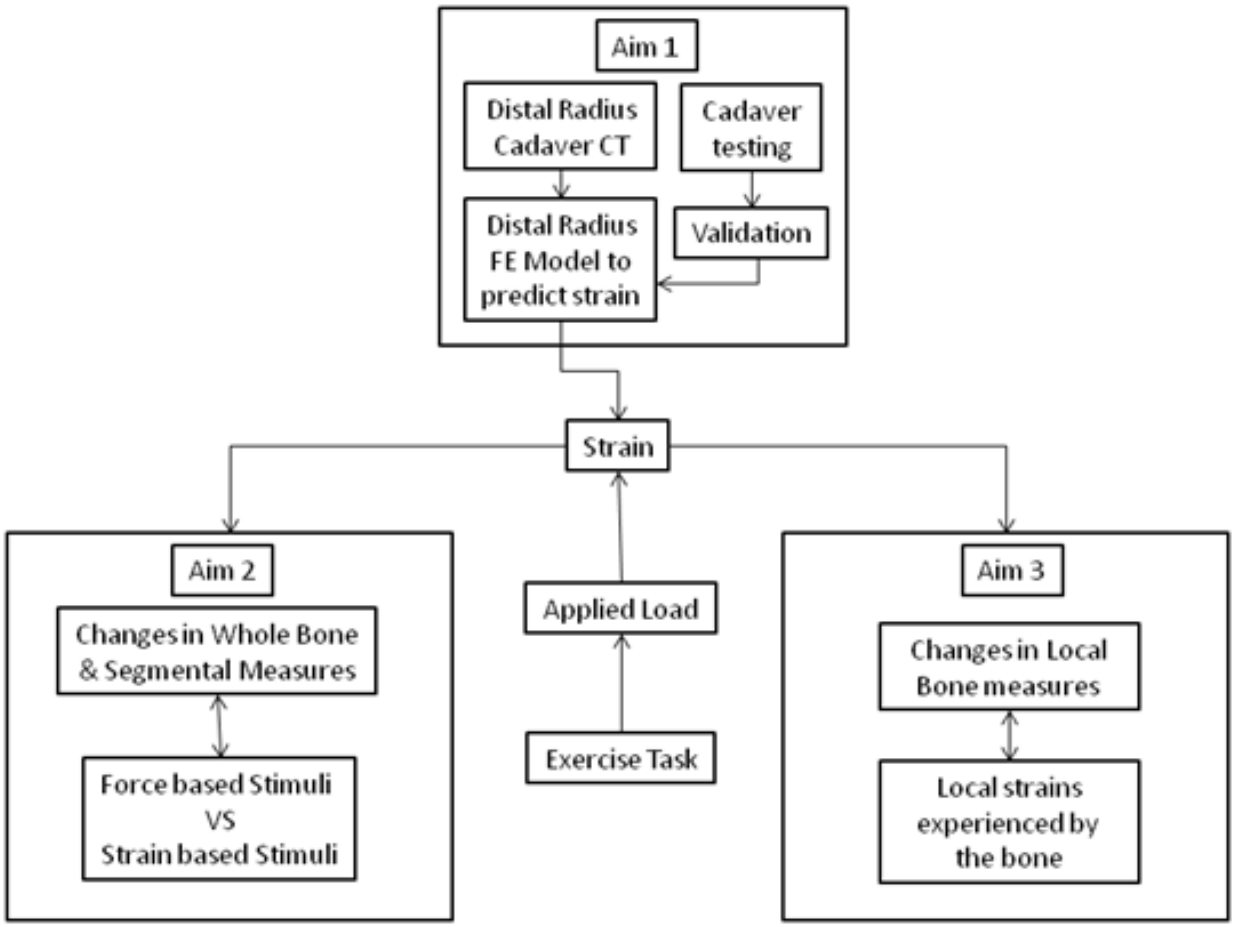

Figure 1-2: Experimental design

Chapter 2. Literature Review

2.1 Bone Adaptation Theories

Wolff is credited with the general theory of bone adaptation. **Wolff's law states that any change in the form and function of bone is followed by a certain definite alteration in its internal architecture and external conformation** (Wolff, 1892). The law suggests that bone attains optimal configuration, i.e. maximum structural efficiency with minimum mass, and that its structure can adapt in response to a changing mechanical environment. Prior to Wolff, Roux suggested that **apposition and resorption by bone cells determined the changes in bone, and its activity is modulated by mechanical stress (**Roux, 1881). Koch analyzed the structural properties of a human femur using the general principles of applied mechanics and graphic statistics to show that the trabeculae were oriented along the principal stresses (Koch, 1917). He suggested that **bone density would be higher in areas of high shear stress and concluded similar to Wolff that bone attains maximum strength with minimum mass.** Pauwels expanded on this theory to describe the effects of mechanical stresses on long bone cross-section and fracture healing (Pauwels, 1980).

Glucksmann used skeletal tissue from chick embryos, cultured in such a way that as they grew, different amounts of tensile stresses were developed. He found that **increased tension increased the rate of bone formation while reduced tension diminished ossification, and concluded that mechanical tensile stress stimulates osteogenesis *in-vitro*** (Glucksmann, 1942). Frost was the first to theorize how bones adapt to alterations in the mechanical environment (Frost, 1964). He determined that bone adapted through modeling and remodeling, and can be attributed to the individual or coupled action of osteoblast and osteoclast cells.

Additionally he suggested that not only was mechanical strain the principal determinant of bone adaptation, but that a minimum threshold must be surpassed before bone adaptation could occur. Frost theorized that **the response of bone to its mechanical environment is controlled by a "mechanostat" that regulates bone functional adaptation.** He suggested that below a certain threshold of mechanical signal, bone is resorbed, and is therefore rid of excess mass. Above another threshold, wherein bone is exposed to loads greater than typical, bone formation occurs to increase bone strength.

Osteocytes have been postulated as mechano-sensors (Bonewald, 2006). Tissue deformed by mechanical loading generates fluid pressure gradients resulting in interstitial fluid-flow in the lacunae and canaliculi. This fluid flow perturbs the osteocytes and their dendrites and plays a role in sensing and transduction of the mechanical signal to a biochemical signal resulting in bone formation. In case of lower than typical forces, such as disuse, osteocyte apoptosis acts as the mechano-transduction process and results in resorption. Remodeling, i.e. the coupled action of osteoclasts and osteoblasts (resorption and formation) is generally attributed to osteocyte apoptosis caused due to micro-damage accumulation. Remodeling prevents the accrual of excessive micro-damage while gradually altering bone strength and ridding the bone of excess mass.

These theories have been used as the basis for the experimental study of mechanically mediated bone adaptation. Animal, human, and computational models have been used to better understand and predict adaptation behavior of bone in response to mechanical stimulus.

2.2 Animal loading models

Animal models have been valuable tools for understanding the process of bone adaptation, and have been studied with the long term goal of developing mechanical loading-based interventions to improve bone strength in humans. Animal models have been extensively used to gain *in-vivo* data of how the bones react to loading in a very controlled environment and time-span. Additionally, a more direct quantification of applied mechanical stimulus and adaptive response is possible with animal models.

Dynamic loads initiate bone formation, while static loads lead to bone resorption. This observation was first made when controlled dynamic or static bending loads were applied to isolated ulnae of turkeys (Lanyon and Rubin, 1984). Statically loaded bones showed a 13% decrease in cross sectional area, whereas the dynamically loaded bones showed a 24% increase in cross-sectional area predominantly caused by bone deposition at the periosteal surface. Using the same loading model, the authors showed that the change in the ulna cross-sectional area increased with an increase in applied strain (Rubin and Lanyon, 1985). A four-point bending model of rat tibia showed similar results, the percent new bone formation increased with increase in applied strain (Turner, 1991). The author also observed **that bone formation rate at the rat tibia increased with increase in loading frequency** (Turner, 1994).

Adaptive response of bone depends not only on the magnitude of the load, but also on age. The tibiae of 8 week, 12 week and 20 week old mice were loaded to peak loads of 2 N to13 N at 2 Hz with a 10 second rest between cycles, for 40 cycles/day, 3 days a week for 2 weeks (De Souza, 2005). A load magnitude related increase in new cortical bone formation was observed for forces above 8.7 N. Additionally, new bone formation was significantly lower in 12 week and 20 week old mice than the 8 week old mice. Architectural changes in trabecular

organization varied with age; the 8 week old mice showed a significant increase in bone volume fraction, whereas the 12 and 20 week old mice showed a significant decrease.

Repeated loading may desensitize osteocytes making the bone less responsive to loading. Insertion of a rest period between loading cycles may help in re-sensitizing the cells (Srinivasan, 2002). The left ulnae two year old turkeys were subjected to 100 loading cycles of saw tooth waveform at 1 Hz in bending, inducing a peak normal strains of about 800 με. The turkeys were divided into two groups, one no rest between cycles, and one with a 10 second pause between cycles. Although the percent periosteal-labeled surface was significantly elevated in the loaded ulna of both the loaded groups compared with the contra-lateral ulna, the loaded ulnae of the rest inserted group showed a significantly higher percent periosteal-labeled surface compared to that of the standard group. In the same study, 10 week old female mice were also used. The right tibiae of these mice were externally loaded using a non-invasive murine tibia loading device. The mice were divided into 3 groups, a low magnitude group (100 cycles a day, 0.25N peak load using a 1Hz trapezoidal waveform for 5 consecutive days), a low magnitude rest inserted group (same wave form as low magnitude group for 10 cycles a day with 10 sec pause inserted between cycles) and a high magnitude group (same as low magnitude group but with 0.5 N peak loads). The loaded tibia of the low magnitude with rest inserted group showed a significantly elevated periosteal bone formation rate and was equivalent to the bone formation response of the high magnitude protocol. In another study, five-week-old rats were divided into control and five jump training groups comprised of 5, 10, 20, 40, and 100 jumps per day, 5 days a week, for 8 weeks (Umemura, 1997). Significant increases in cortical cross-section area, and fracture force were observed for the 5-jumps per day group, and only small differences in morphological and mechanical parameters between the 10-, 20-, and 40-jumps per day groups.

Mechanical loading induces a site specific bone adaptation response. A non-invasive murine tibia axial-loading model was used to study the effects of loading on adaptation of long bones, quantified after 2 weeks and 6 weeks of loading (Fritton, 2005). The tibiae of adolescent 10 week old C57BL/6 mice were compressed with a peak to peak strain magnitude of 800 με for 1200 cycles per day, 5 days a week. A significant and site specific increase in mineral content was observed, with a greater response in the proximal cortico-cancellous region than the cortical midshaft. A significant increase in the maximum cross sectional moment of inertia was observed at 25% of the length of the bone. Significant increase in bone volume fraction was observed at both 2 and 6 week loading, but the increase in trabecular thickness was significant only after 6 weeks of loading.

The site specific bone adaptive response may be related to the strain, or strain gradient magnitude. An isolated turkey ulna loading model stimulated periosteal new bone formation, and the locations of the new bone formations were highly correlated with peak magnitudes of strain gradient (Gross, 1997).

It is likely that **bone responds to these regions of high strains to reduce the peak strains, and that the adaptive response maybe dependent on strain rather than force.** When digital image correlation was used to measure bone surface strains during axial loading of murine tibiae (Sztefek, 2010), a more uniform strain distribution was observed in the tibiae that had previously been mechanically loaded, suggesting that adaptation occurred to reduce peak strains.

Several other modes of loading have been utilized to explore the relationship between bone adaptation and mechanical signals. These include whole body vibrations (WBV), bending loads, and fatigue loading, in addition higher loads at low frequency, Eight week old mice were

divided into age matched controls, whole body vibrations (WBV), and WBV with rest groups (Xie, 2006). The loaded groups were subjected to high frequency low-level mechanical vibrations of 45 Hz, 0.3g for 15 min a day, 5 days a week for 3 weeks. The rest inserted group was subjected to a rest period of 10 sec after every 1 sec of vibrations. The mechanical vibrations induced peak strain magnitude of 10 με on the surface of the proximal tibia. Osteoclastic activity in the trabecular metaphysic and epiphysis was significantly lower, and the bone formation rates on the endocortical surface of the metaphysic were significantly greater, in WBV group than in age matched controls. The rest insertion failed to enhance these differences. The data indicated that in a growing skeleton, **daily short periods of low magnitude high frequency mechanical vibrations can inhibit trabecular bone resorption and increase bone formation.**

A three-point bending protocol, and a transverse loading protocol were compared in osteoporotic (SAMP6) and control (SAMR1) mice, aged 4-5 months **(**Silva, 2008); the mice were loaded to strains of either 1000 με or 2000 με for 2 weeks. At the end of 2 weeks, histomorphometric analysis were carried out, and significantly increased mineralizing surface was observed in loaded vs. non loaded tibiae in both type of mice. Endocortical bone formation was observed with three-point bending; however, there was no evidence of increased endocortical bone formation due to the two-point transverse loading, suggesting that **bending is required for endocortical response.**

A fatigue loading protocol using adult female rats were utilized to study the effects of bone adaptation on the fatigue resistance of bones (Warden, 2005). The rat ulnae were axially compressed for 360 cycles a day, 3 days a week for 5 consecutive weeks, at 2 Hz. Significant changes in the bone geometry of the loaded ulna were observed compared to the control. The loaded ulnae required more than 100 times the number of cycles to failure compared with the

non-loaded ulnae. **Fatigue resistance increased due to bone adaptation**, **and was attributed to the enhanced structural properties of the bone.**

Although the different animal loading models incorporate different loading strategies with varying peak loads and frequencies, they all result in quantifiable changes in bone content and bone structure. This is because mechanically induced bone adaptation likely depends on some fundamental rules (Turner, 1998). a) It is **driven by dynamic rather than static loading and increases if the magnitude and/or frequency of the dynamic signal is increased**. b) Beyond some point, increased loading duration does not yield an increased bone mass. **As the duration of loading increases, the bone formation response tends to saturate**. c) Bone adaptation is error-driven. **Bone cells accommodate to routine mechanical strains, and respond to abnormal strain changes.** Since bone is fundamentally similar between species, these rules should also apply to bone adaptation in humans; however, the specific manner in which these factors affect human bone may be different.

2.3 Human loading models

Athletic populations participating in high- or odd-impact sports have been observed to have higher BMD and physically larger bones (Nikander, 2005). Ducher et. al (Ducher, 2005) used quantitative magnetic resonance imaging to quantify bone geometry in response to playing tennis. Long-term tennis players were recruited and bone geometrical parameters of the radius of the dominant arm were compared to those of the non-dominant arm. Significant structural and mineral differences were observed with higher bone volume, BMC, and BMD on the dominant side. The study suggested that in addition to muscle contraction, the mechanical stimuli exerted by the impact have a direct effect on the bone response to tennis playing. In

another longitudinal study, changes in regional and whole body BMD were monitored in gymnasts, runners, swimmers, and controls (Taaffe, 1997). Percent changes in lumbar BMD, and femoral neck BMD were significantly higher in gymnasts than in runners or controls. In addition to the larger changes, the gymnasts also had higher initial BMD values. The results suggested that the high impact differential loading in gymnasts is responsible for the high BMD values characteristic of women gymnasts.

Based on evidence from the above mentioned animal studies, many **exercise-based interventions have been used to maintain and improve bone health, and prevent fall related fractures in older human populations.** A systematic meta-analysis of the effect of training programs on bone mass in older adults (Gomez-Cabello, 2012) indicated that bone-related variables can be increased, or at least a decline in them due to aging attenuated, by following specific training programs, which include walking, strength training, and whole body vibrations. In one such study, post-menopausal women participating in a 6-month exercise program were studied to relate changes in bone structural and mineral properties to the training program (Adami, 1999). The women were divided into an exercise group and a control group. The exercises in the training program were designed to increase stresses at the wrist. Bone structural and mineral parameters were measured before and after the exercise program. Significant increase in cortical BMC and significant decrease in trabecular BMC were observed at the ultra-distal radius of the women in the exercise group. The **increase in cortical BMC was related to the combined increases in the cross-sectional area of cortical bone, and cortical BMD, in response to the increased stress at the wrist.**

Regular high impact exercise may be required for an optimal maintenance of bone health. Healthy pre-menopausal women were assigned into groups performing 0, 2, 4, or 7 days

a week of 50 multidirectional one legged hops, for a period of 6 months (Bailey, 2010), and DEXA measured BMD assessed at the femoral neck at the start and the end of the training protocol. The change in BMD at the femoral neck of the exercise limb differed between groups. Daily exercise significantly increased femoral neck BMD, but less frequent exercise had no significant effect, suggesting regular high impact exercise may be required to reduce hip fragility.

One major challenge in working with humans is the inability to directly measure strain experienced by the bone. Force measures have been widely used as an alternate measure of mechanical stimulus experienced by the bone. In addition, **accelerometers have also been used with some success to obtain a surrogate measure of mechanical stimulus.** Physical activity of healthy women in a 12 month high-intensity exercise program was continuously monitored using a waist worn accelerometer (Ahola, 2009). DEXA and QCT measured bone structural and mineral parameters at the proximal- and mid-femur were measured at baseline and at the end of the exercise program. The physical activity data obtained from the accelerometer was found to be positively correlated with 12 month changes in femoral bone parameters.

Measures of mechanical stimuli have also been obtained from physical activity and history surveys and questionnaires. The Bone Loading History Questionnaire (BLHQ) has been developed to assess loads applied to the skeleton in bone loading units and have been correlated with femoral neck areal BMD (Dolan, 2005). The Historical Leisure Activity Questionnaire (HLAQ) (Kriska, 1988) has been successfully used to show that long-term participation in sport and weight bearing activities has a region-specific cortical bone mass and density adaptations in the lower limbs (Bailey, 2010). The Bone-Specific Physical Activity

Questionnaire has been observed to predict bone strength at skeletal sites at risk of osteoporotic fractures (Weeks, 2008).

The above studies have related exercise-based mechanical stimuli to bone adaptation, however these use indirect measures, such as force, accelerations, and questionnaires, to quantify the mechanical stimuli. These do not truly describe the *in-vivo* mechanical environment experienced by the bone during the mechanical stimuli, and may yield in ambiguous findings. For example, although Bailey et.al observed increased femoral neck BMD in response to regular hopping (Bailey, 2010), another study indicated that continuous bilateral hopping exercise was ineffective in initiating bone response in healthy elderly men (Rantalainen, 2011).

Non-invasively quantifying the *in-vivo* mechanical environment experienced by the bone, as well as its response to the stimulus, is not trivial. Direct methods of measuring the mechanical stimuli, such as using strain-gauged bone staples, have been used to measure *in-vivo* strains and strain rates at the distal-radius during activities of daily living (Foldhazy, 2005). However, these methods are often impractical and invasive.

2.4 Finite Element Models

Finite element modeling, which is a computational modeling technique, has been successfully used to predict the *in-vivo* mechanical environment of bone during a mechanical stimulus or task. Finite element method (FEM) is a numerical technique used to find approximate solutions to boundary condition problems. The method originated with the need to solve complex elasticity and structural analysis in fields of civil and aeronautical engineering, and its first demonstrated use in skeletal mechanics was in 1972 (Brekelmans,

1972). Using FEM, a complex structure of interest can be discretized into a finite number of sub-structures of a simpler geometrical shape called elements, and laws of equilibrium used to solve material and structural analyses at each element. FEM is advantageous in the evaluation of mechanical behavior of the musculoskeletal system because (a) it is non-invasive, (b) reconstructs the mechanical behavior at multiple sites of the tissue, and (c) it is capable of solving complex geometrical and loading conditions.

With the advent of inexpensive computational power, practical application of three-dimensional FE models has expanded. A three-dimensional voxel based FE modeling method was developed and validated to accurately characterize the strains on the surface of the diaphysis and neck of a femur with the femoral head loaded in compression (Keyak, 1990 and Keyak, 1993). The results of the analyses showed significant relationships between measured and predicted strain ($r = 0.769$) and a standard error of estimate of 254με.

More recent studies have used geometry based meshes in subject-specific FE models to obtain stronger and more accurate relationships between measured and predicted strains. A FE model mesh generated using tetrahedral elements, assigned inhomogeneous material properties to the elements based on the CT Hounsfield Unit values, was validated using experimental strain gage data (Schileo, 2007). The results showed that the model predicted the experimental strains with high accuracy ($R^2 = 0.91$, RMSE = 9.8%, peak error = 60.6%). Fine FE meshes of cadaveric tibia were used to predict strains under multiple loading conditions, for intact and artificial knee implanted tibiae (Taddei, 2008). The predicted strains were compared to cadaveric strain gage data for the same specimen. The model was capable of accurately predicting the strains with a $R^2 = 0.98$, RMSE = 6% for the intact tibia, and $R^2 = 0.97$, RMSE = 8.8% for the implanted tibia. A FE model of the distal radius was generated using hexahedral

elements, and was validated with cadaveric strain data (Edwards, 2012). The model predicted strains (r = 0.9, RMSE = 13% of peak measured strain), and fracture strength (mean absolute percent error = 11.6%) with considerable accuracy.

2.5 Mathematical models of adaptation

As discussed earlier in this chapter, bone adaptation has been related to magnitude, and frequency, of the applied load, as well as duration and number of bouts of the loading. Many of these relations have been described in mathematical forms (Turner, 1998). Additionally, **mathematical models based on a combination of these relationships, and empirical data have been developed to predict bone's adaptive response to applied mechanical stimulus.** A mathematical formula was proposed to combine the attributes of a mechanical stimulus, as a single parameter, daily loading stimulus (DLS) (Carter, 1987). The daily loading stimulus was expressed in terms of effective stress (Equation 2.1) or effective strain (Equation 2.2).

$$DLS = \left[\sum_{j=1}^{k} N_j \sigma_j^m\right]^m \qquad \text{Equation 2.1}$$

$$DLS = \left[\sum_{j=1}^{k} N_j \varepsilon_j^m\right]^m \qquad \text{Equation 2.2}$$

where k is the number of different activities, N is the number of cycles for the corresponding activity, m is an empirical constant, and σ is the stress and ε is the strain associated with the activity.

This theory was expanded on to develop a unified, time dependent theory for periosteal, and internal modeling and remodeling (Beaupre GS, 1990). The authors used an idealized remodeling curve (Figure 2-1) to derive a relation between bone apposition/resorption rate (ṙ), and the daily stress stimulus (ψ́) (Equation 2.3):

$\acute{r} =$ Equation 2.3

$$c_1(\varphi_b - \varphi_{bAS}) + (c_2 - c_1)w_1(\varphi_b - \varphi_{bAS}) < -w_1$$

$$c_2(\varphi_b - \varphi_{bAS}) - w_1 \leq (\varphi_b - \varphi_{bAS}) < 0$$

$$c_3(\varphi_b - \varphi_{bAS})0 \leq (\varphi_b - \varphi_{bAS}) \leq +w_1$$

$$c_4(\varphi_b - \varphi_{bAS}) + (c_3 - c_4)w_2(\varphi_b - \varphi_{bAS}) > w_2$$

where ψ_b is the tissue level stress stimulus, ψ_{bAS} is the attractor state stress stimulus, c_1, c_2, c_3, and c_4 are the empirical rate constants, and w_1, and w_2 is the width of the normal activity region.

Equation 2.3 can be directly used to calculate external bone remodeling, however to calculate internal remodeling, the authors derived a relation based on the surface area density (S_v) (Equation 2.4):

$\rho = \acute{S}_v \acute{r} \rho_t$ Equation 2.4

where ρ is the time rate of change of the apparent density and ρ_t is the density of fully mineralized tissue.

These and related models have been tested using idealized data, as well as experimental studies. To demonstrate the practical applications of the daily stress stimulus, the density distribution within a 2-dimensional, idealized adult proximal femur under an assumed normal loading history was calculated using the theoretical model (Beaupre, 1990). Beginning with a homogenous distribution of bone, a density distribution similar to previously documented observations was attained using the theoretical model. The daily strain stimulus theory was used

to quantify bone overloading and hypertrophy using data from multiple experimental animal studies (Chen, 2010). The authors observed that bone apposition rate increased with increase in the daily strain stimulus, and suggested that the theory could be used to consistently predict bone apposition rates, and used to improve the design of future bone loading studies. The validity of the daily stress stimulus theory was tested using the strain histories at the ulnae of turkeys (Adams, 1997). The study suggested that apart from magnitude and number of the applied stimulus, certain other attributes such as frequency, rate, and spatial gradient may also be needed to accurately predict bone adaptation. Energy equivalent strain calculated from *in*-vivo strain gage data was used to obtain the daily strain stimulus at the antero-medial human tibia during walking and jogging (Mikic, 1995). This study was the first to incorporate experimentally based strain studies in humans with computational models of functional adaptation. An enhanced daily load stimulus (EDLS) theory was developed taking into account saturation and recovery of the osteogenic potential of bone adaptation as well as standing (Genc, 2009). The authors developed the EDLS model with the aim of applying it towards the prescription of exercise to crewmembers on long-duration space flight.

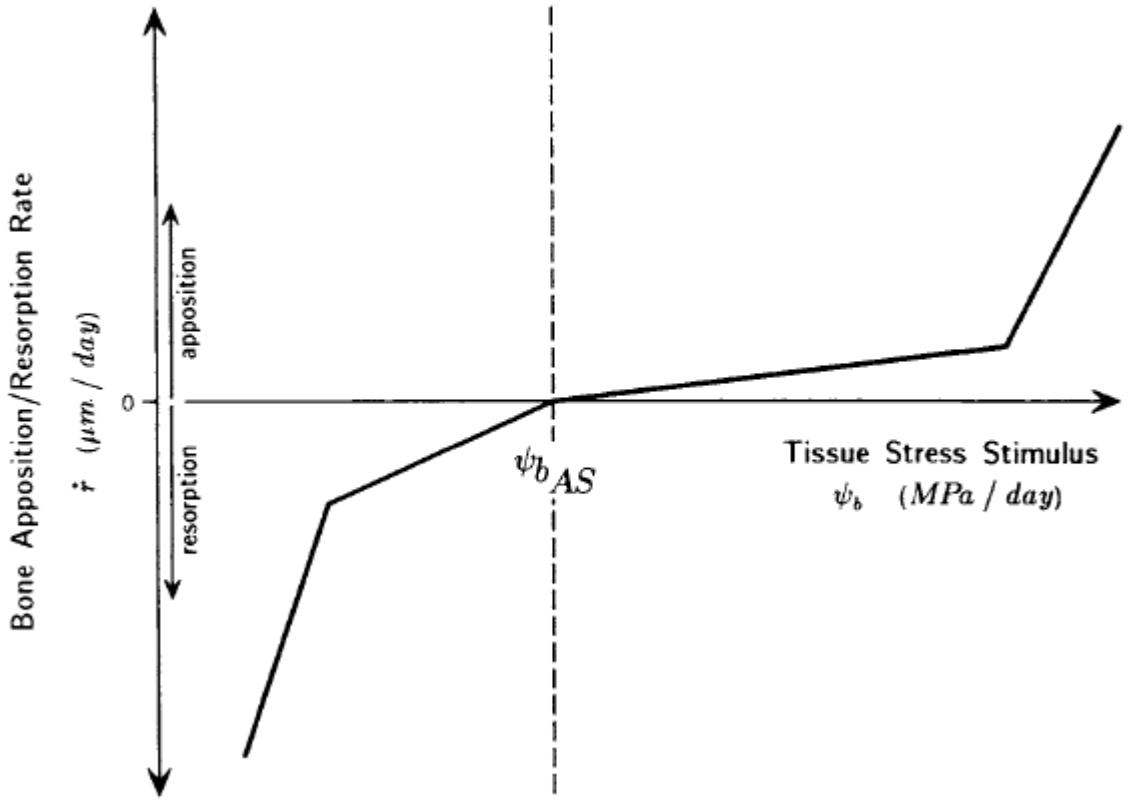

Figure 2-1: Idealized linear bone apposition/resorption rate (Beaupre, 1990)

Chapter 3. Aim1

Create methods for subject specific finite element models used to predict surface strains at the distal radius during an exercise task, and validate the methods with cadaveric testing.

3.1 Introduction

Fractures of the distal radius are a common consequence of falls in older adults (Vogt, 2002). Exercise based interventions have been used to maintain and improve bone strength and prevent fall related fractures in older populations (Gomez-Cabello, 2012), based on evidence that bone adapts to the mechanical environment it experiences. The relationship between mechanical environment and bone adaptation has been well described in a variety of animal models (Turner, 1991; Gross, 1997). These studies have shown that mechanical loads above a minimum strain threshold initiate bone adaptation. Mechanical strains have been used with theoretical models of functional adaptation such as the Daily Stress or Strain Stimulus theories that define a theoretical relationship between mechanical strain stimuli and bone adaptation.

In humans, exercises have been shown to increase bone mineral and mechanical properties (Bailey, 2010). However, a direct relation between the adaptation response and the strain environment has not been quantified in humans. This is in part due to the difficulties in quantifying the strain environment of a bone during an exercise task. External reaction forces are often used as a surrogate measure of strain. However, the relationship between external force and mechanical environment within the bone is complex. In addition to any applied forces (external and muscle contraction), this mechanical environment is also affected by the size and shape of, and mineral distribution within the bone. Strain is a more direct measure of the mechanical environment experienced by the bone. The ability to measure or accurately predict bone strains

non-invasively is important in the development and evaluation of exercise regimes to improve bone health and reduce the occurrence of fractures.

Subject specific finite element models have been successfully used to predict bone strains (Keyak, 1993; Edwards, 2012). However, the accuracy of such models is dependent on the equations chosen to relate bone's density to its modulus (Schileo, 2007). We have developed a novel *in-vivo* loading model to study the interaction between mechanical loading and bone adaptation in humans (Troy, 2103). The loading task involves leaning on to the palm of the hand to apply an axially directed force through the distal radius (Figure 3-1a). The objective of this study was to create and validate methods for subject specific finite element model generation, which will be used to predict the surface strains experienced by the distal radius during this loading task. This was accomplished by using quantitative computed tomography (QCT) data and cadaveric testing of the distal forearm. The cadaveric testing was performed under loading conditions simulating the mechanical loading task of interest mentioned above. The experimentally measured surface strains at the distal radius were also used in conjunction with the Daily Strain Stimulus Theory (Mikic, 1995) to calculate a single local parameter reflecting the total stimulus acting on the bone.

3.2 Methods

3.2.1 Specimens

Four female cadaveric forearms with hand intact (mean age 86.75 years, range 82–89 years) obtained through anatomical gift, freshly-frozen and stored at −20 ◦C were used for this study. The specimens were thawed to room temperature for: 1) CT data acquisition; 2) specimen dissection and potting; and 3) strain gage application and mechanical testing. The distal most 12

cm of the forearms were imaged with a clinical CT scanner (BrightSpeed; GE Medical Systems, Milwaukee, WI, 120 kV, 180 mA, voxel size: 0.234 mm X 0.234 mm X 0.625 mm). A calibration phantom (QRM, Moehrendorf, Germany) with calcium hydroxyapatite equivalent concentrations of 0, 400, and 800 mg/cm^3 was used to establish the following averaged linear relationship between CT Hounsfield units (Hu) and calcium hydroxyapatite equivalent density (ρha) in g/cm^3:

$\rho_{ha} = 0.0069 + 0.0007*Hu$ (r^2=0.9993)

3.2.2 Specimen preparation

Soft tissue proximal to the wrist joint capsule was removed and a radio-ulnar osteotomy performed 14 cm proximal to the distal dorsal tubercle. The proximal most 8 cm of the forearms was potted in polymethyl methacrylate (PMMA). With the periosteum removed, surface sanded, and cleaned with isopropyl alcohol, six rectangular strain gage rosettes (TS1N-K120M-PK06-LE, Micro-Flextronics Ltd, Coleraine, N. Ireland) were adhered circumferentially to the periosteal surface using cynoacrylate glue. Three rosettes were mounted distally just proximal to the distal dorsal tubercle and three were mounted 3 cm proximal to these gages (Figure 3-1b). The two locations were chosen to measure a range of periosteal strains. The distal location is comprised primarily of trabecular bone whereas the proximal location is comprised primarily of cortical bone.

a)  b) 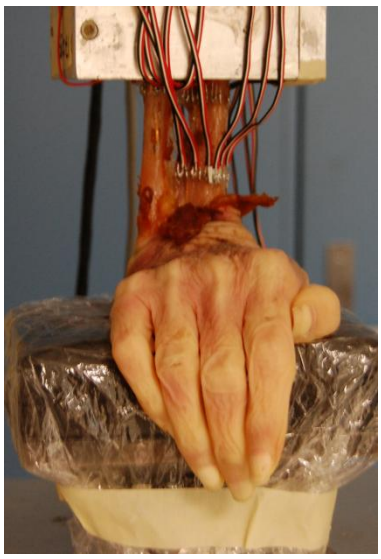 c) 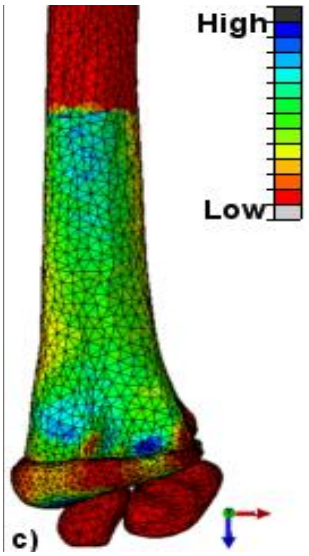

Figure 3-1: a) Targeted loading protocol, b) Experimental testing setup, c) Minimum Principal Strain map of the finite element model.

3.2.3 Mechanical testing

Specimens were aligned on a uni-axial materials testing machine (MiniBionix 858, MTS Systems, Eden Prairie, MN) so as to mimic the loading environment of the loading task (Figure 3-1b). The actuator was driven at a fixed displacement rate of 0.3 mm/sec until a load of 300 N was reached. Force, displacement, and six analog channels (recording strain information corresponding to two rosettes) were concurrently collected at 100 Hz. Five repeat trials were collected for each rosette resulting in a total of 15 tests.

3.2.4 Strain gage location

For each specimen, reflective markers were attached at each strain gage location and at three anatomical landmarks: the distal dorsal tubercle, the styloid process of the radius, and the

palmar surface of the distal radio-ulnar attachment on the palmar side. Three additional markers were attached on to the PMMA block. An eight camera motion capture system (Motion Analysis, Santa Rosa, CA) was used to take a static 3D capture of the locations of these markers. The positions of the markers were used to obtain the locations of the strain gages relative to the anatomical locations. An eight camera system similar to the one used here has been shown to have an accuracy of more than 99.3% and a resolution of 0.6 mm or better for a static capture (Kertis, 2009).

3.2.5 Model generation

To determine the optimal mesh and model parameters, mesh size (element size), cartilage material property, and density-elasticity relationships were varied. Initially, convergence analysis was performed on the mesh size, by keeping the cartilage and bone material properties constant. Once the optimal mesh size was determined, three cartilage material properties were tested keeping bone material properties and mesh size constant. And finally, using the optimal mesh size and cartilage material properties, four density-elasticity relationships were tested by comparing the predicted strain values with the corresponding values obtained from the cadaver tests.

Segmented CT data were used to create finite element geometry of the radius, lunate and scaphoid using the Mimics Innovation Suite v15.0 (Materialise, Leuven, Belgium). The space between the distal surface of the radius and the lunate and scaphoid bones was defined as the cartilage (thickness = 1.4±0.4 mm). The articulating surface was created by expanding the distal most surface of the radius, and subtracting out the voxels intersecting the carpal bones, thereby creating a seat for the carpal bones. The segmented geometries were exported in to 3-matic v7.0

(Materialise, Leuven, Belgium), and a quadratic tetrahedral element mesh was generated for each specimen. Maximum triangle edge length and maximum geometrical error was adjusted for the radius to obtain average element volumes of 0.25 mm^3, 0.5 mm^3, 0.75 mm^3, or 1.25 mm^3. For all models, the scaphoid and lunate were meshed with an element volume of 0.5 mm^3, and the cartilage was meshed with an element volume of 0.25 mm^3. The cartilage mesh was more refined compared to the scaphoid and lunate meshes so as to obtain a more stable contact between the cartilage and the carpal bones. Convergence analysis was performed for each specimen using these element sizes.

The cartilage was defined as either i) a linear elastic material with a modulus of 10 MPa and a Poisson's ratio of 0.45, ii) a linear elastic material with a modulus of 50 MPa and a Poisson's ratio of 0.45, or iii) a neo-Hookean hyperelastic material with a modulus of 10 MPa and a Poisson's ratio of 0.45 which was based on published literature (Anderson, 2005; Armstrong, 1984). The scaphoid and lunate were defined as non-deformable rigid bodies. The radius was assigned non-homogenous linearly-isotropic material properties based on four previously established density-elasticity relationships:

$E=10{,}500\rho_{ash}^{2.25}$ (Keller, 1994) (i)

$E=2{,}500\rho_{app}^{3}$ (Carter and Hayes, 1977) (ii)

$E=6850\rho_{app}^{1.49}$ (Morgan, 2003, femoral specimens) (iii)

$E=8920\rho_{app}^{1.83}$ (Morgan, 2003, pooled specimens) (iv)

where E is the modulus expressed in MPa, ρ_{ash} (ash density) and ρ_{app} (apparent density) expressed in g/cm^3. Calcium hydroxyapatite equivalent density (ρha) was converted to ρ_{app} and ρ_{ash} using:

$\rho_{app} = \rho_{ha}/0.626$ (Dalstra, 1993), $\rho_{ash} = \rho_{app} * 0.6$ (Schileo, 2008)

The element densities were calculated as the mean density of the voxels enclosed in the element. The material properties were binned into 200 bins corresponding to about 150 MPa each, based on preliminary analyses, and assigned a Poisson's ratio of 0.4 (Reilly, 1975; Keyak, 1993). Density values less than 0.01 g/cm^3 were reassigned a density value of 0.01 g/cm^3. To account for partial volume effects, the material assignment was based on an area corresponding to the segmented radius that was eroded by 1 voxel. Any elements that were entirely outside this area were assigned a uniform density of 1.2 g/cm^3.

The models were exported in to Abaqus 6.10 (Simulia, Providence, RI) for setup and analysis. The proximal part of the radius corresponding to the potting location was fully constrained. The scaphoid and lunate were then rotated in the anterior-posterior direction by 70° and 53° to simulate a wrist extension of 80°. These rotations were based on carpal bone kinematics as a function of wrist angle (Moojen, 2002; Kobayashi, 1997; Wolfe, 2000). Contact was modeled between the surfaces of the cartilage and scaphoid, and cartilage and lunate. During loading, the radio-carpal ligaments and the wrist joint capsule were assumed to keep the carpal bones seated within the cartilage. Hence, a tied interface contact model was defined wherein the carpal bones were not allowed to slide once they were in contact and seated into the cartilage. Additionally, the carpal bones were not allowed to rotate once they were in contact with the articulating surface. The loading simulation was divided into two steps, 1) Displacement step:

The carpal bones were displaced vertically towards the radius until contact was established, and the reaction force was about 10 N and 2) Load step: A static ramped force of 300N was applied to the centroid of the scaphoid (180N) and lunate (120N) based on the assumption that 60% of the load transmitted through the wrist is borne by the scaphoid (Majima, 2007; Schuind, 1995;). The line of action of the resultant force vector was determined for each specimen using an unsymmetrical beam theory analysis based on proximal strain gage and CT information (Edwards, 2012).

3.2.6 Daily strain stimulus

The Daily Strain Stimulus (ξ) was calculated using the strain gage data from cadaveric experimentation, based on the following equations (Mikic, 1995):

$\xi\ (\mu\varepsilon/day) = [\Sigma n \Delta E_e^{\,m}]^{(1/m)}$

n = number of loading cycles per day, m = an empirical constant (m=4), Ee = energy equivalent strain ($\mu\varepsilon$),

$E_e = (1.16\varepsilon_1^{\,2} + 0.72\varepsilon_1\varepsilon_2 + 0.79\varepsilon_2^{\,2} + \gamma_{12}^{\,2})^{0.5}$, and ε_1, ε_2, and γ_{12} are the strains in the principal material direction.

The Daily Strain Stimulus was calculated for each specimen at each strain gage location as well as for the entire section. The strain used to calculate the daily strain stimulus for the entire section was averaged from the strains obtained from the strain gages using a power mean formula strain= $[\Sigma\varepsilon^4/n]^{1/4}$,

where ε = strain, n = number of strain gages

3.2.7 Data analysis

Maximum and minimum principal strains were calculated for each rosette at the target load of 300N. The between trial repeatability of the principal strains was examined using interclass correlations (ICC). The strain map for a sample FE model is shown in Figure 3-1c. For convergence analysis, whole model strain energy density (SED), magnitude of peak displacement, and principal strains for a 5 mm sectional the ultra-distal region were calculated for each of the element sizes for all specimens, and plotted versus the corresponding number of elements. To determine the sensitivity of the model to cartilage material properties, mean maximum (E_{max}) and minimum (E_{min}) principal strains were calculated for a 5mm section at the ultra-distal radius for each of the cartilage material properties for all specimens.

To determine the density-elasticity relationship that best predicted experimentally measured strains, model predicted strains were compared to the experimentally-measured strains. Predicted strain values at the elements corresponding to each rosette location were transformed into the local surface co-ordinate system. Maximum and minimum principal strains were calculated at the surface, and the values were averaged for all elements within each rosette location. The rosette's had an active gage area of 6.2 mm^2 and corresponded to about 8 elements. These model-predicted and experimentally-measured principal strains were then compared using Pearson's r, linear regression, root mean square error (RMSE), and maximum error. The density-elasticity relationship resulting in the highest correlation, and lowest error were used in the validated models. Means and standard deviations of the Daily Strain Stimulus were calculated for each ultra-distal strain gage location, and for the entire ultra-distal section containing the strain gages.

3.3 Results

3.3.1 Mechanical testing

The testing was highly repeatable. The ICC for maximum principal strain at 300N measured over five trails was 0.996 ($p<0.0001$), and the ICC for minimum principal strain over 5 trails was 1.000 ($p<0.0001$). The mean principal strains calculated at each of the strain gage locations are shown in Table 3-1.

Table 3-1. Mean, standard deviation, and range of principal strains calculated from the cadaver testing. Reported values are in micro-strain (με).

Gage Location	**Emax**			**Emin**		
	Mean	SD	Range	Mean	SD	Range
Distal Dorsal thumb	302.4	244.6	(1.5, 604.6)	-1332.7	804.0	(-2600.7, -521.9
Distal Dorsal Ulnar	1143.3	296.2	(777.8, 1426.5)	-1695.3	395.9	(-2172.2, -1261.0)
Distal Palmar	271.7	185.7	(23.3, 438.9)	-102.8	74.3	(-175.4, -8.6)
Proximal Dorsal Thumb	251.6	97.6	(159.4, 343.7)	-293.5	171.6	(-456.1, -130.8
Proximal Dorsal Ulnar	660.3	194.7	(423.3, 879.9)	-1228.0	112.4	(-1361.5, -1101.2)
Proximal Palmar	306.3	93.8	(218.5, 427.7)	-234.5	84.9	(-308.9, -121.4)

3.3.2 Model Convergence

The convergence behavior was analyzed for each specimen. The four element sizes: 0.25 mm^3, 0.5 mm^3, 0.75 mm^3, and 1.25 mm^3, corresponded to 79637 ± 8578, 35508 ± 3375, 24337 ± 1950, and 14264 ± 1024 elements respectively. The convergence behavior for strain energy density versus number of elements is shown in Figure 3-2. Based on these results, an element size of 0.5mm^3 corresponding to 35508 ± 3375 elements was chosen for further validation.

The mean principal strains at 300N were fairly constant for the different cartilage material properties. For cartilage defined as a linear elastic material with E=10 MPa, ν=0.45 the strains were E_{max} = 1225 με and E_{min} = -1876 με, defined as a linear elastic material with E=50 MPa, ν=0.45 the strains were E_{max} = 1150 με and E_{min} = -1817 με, and defined as a hyperelastic material with E=10 MPa, ν=0.45 the strains were E_{max} = 1165 με and E_{min} = -1830 με. Based on these results, and literature review, cartilage was defined as a hyperelastic material with a modulus of 10 MPa, and a Poisson's ratio of 0.45 for further analysis.

3.3.3 Comparison between measured and predicted strains

The scatter plots of predicted versus measured principal strains for the four density-elasticity equations are shown in Figure 3-3. The highest correlation and lowest RMSE between experimentally measured and finite element predicted strain was observed using Eq (iv). These models illustrated an r=0.928 and an RMSE of 424.3 με, with a slope of 0.809 (significantly different from 1), and an intercept of -7.2 (not significantly different from 0) (Table 3-2). One specimen illustrated substantial error (RMSE=713.8 με) relative to the other three specimens and upon further visual examination of the radiographic data, the scaphoid and lunate were observed to be partially fused to the radius and ulna, indicating the possibility of osteoarthritis. Using Eq

(iv), exclusion of this specimen from our analysis resulted in a r=0.968, a slope of 0.984 (not significantly different form 1), intercept of 51.1 (not significantly different from 0), and a RMSE of 219.6 με (11.1% of maximum measured strain).

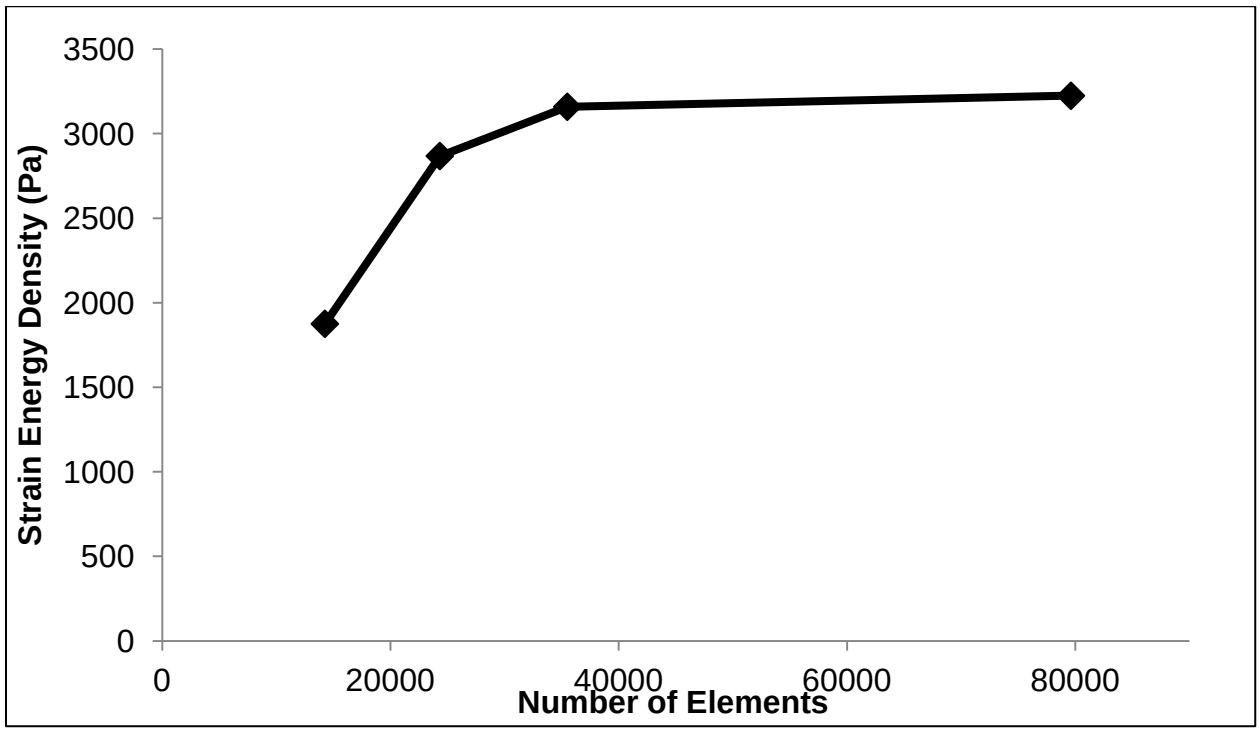

Figure 3-2: Convergence behavior of strain energy density versus number elements, averaged over the 4 specimens. The number of elements corresponded to nominal element volumes of 1.25 mm^3, 0.75 mm^3, 0.5 mm^3, and 0.25 mm^3 from left to right.

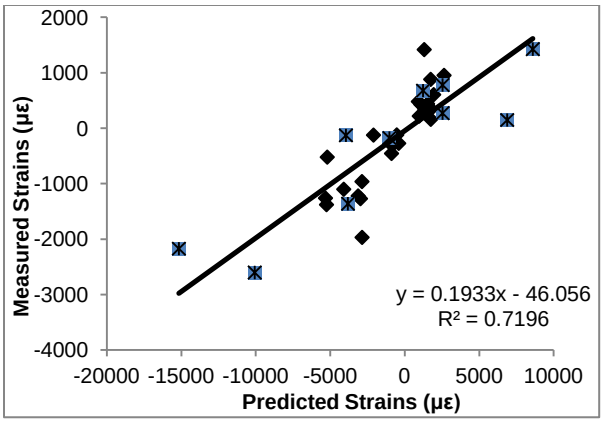

Eq (i)

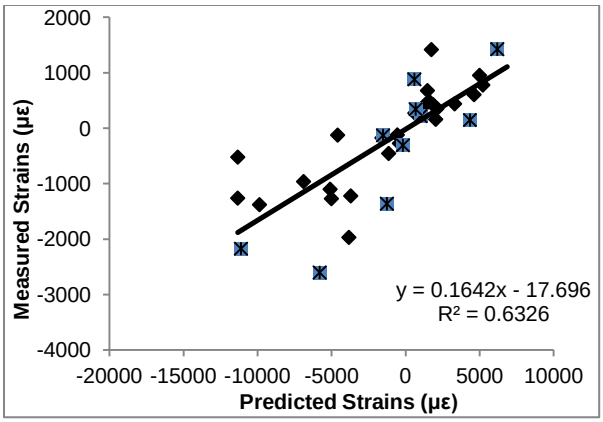

Eq (ii)

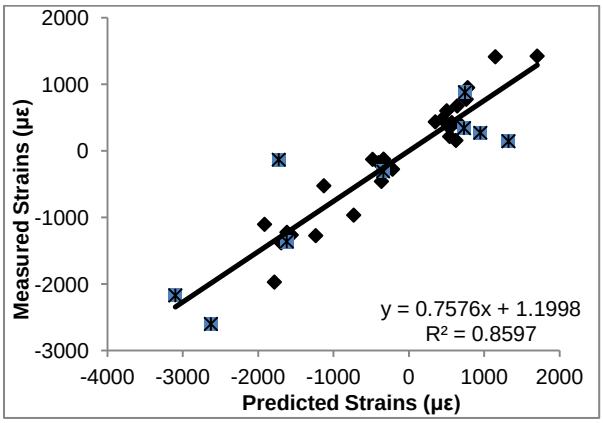

Eq (iii)

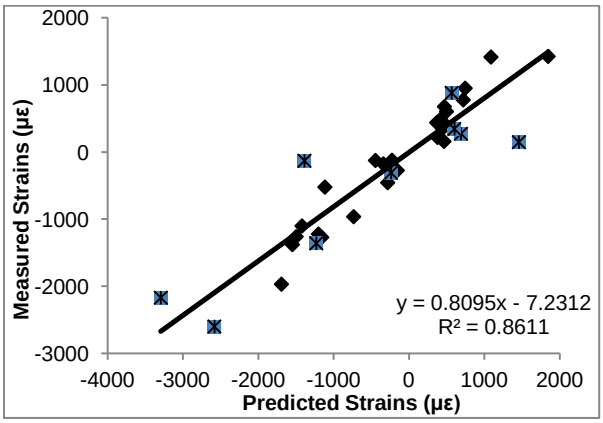

Eq (iv)

Figure 3-3: Scatter plot of predicted versus measured principal strains at 300 N for the 4 density-elasticity equations. Symbols in grey correspond to points of osteoarthritic subject.

Table 3-2: Pearson's r, slope, intercept, root mean square error (RMSE), and RMSE as a percentage of the maximum absolute measured strain, for the four density-elasticity relationships. *[a] Significantly different, [ns] not significantly different from 1 (slope) or 0 (intercept)*

	Eq (i)	Eq (ii)	Eq (iii)	Eq (iv)	Eq (iv) excluding subject with OA
r	0.848	0.795	0.927	0.928	0.968
slope	0.193[a] (CI: 0.151 0.236)	0.164[a] (CI: 0.12 0.209)	0.758[a] (CI: 0.649 0.866)	0.809[a] (CI: 0.694 0.925)	0.984[ns] (CI: 0.874 1.094)
Intercept	-46.1[ns] (CI: -233.1 140.9)	-17.7[ns] (CI: -234 198.6)	1.2[ns] (CI: -132 134.5)	-7.2[ns] (CI: -139.5 125.1)	51.1[ns] (CI: -43.4 145.5)
RMSE (ue)	3557.4	4117.2	472.3	424.3	219.6
RMSE (%)	136.8	158.4	18.2	16.3	11.1

3.3.4 Daily strain stimulus

The daily strain stimulus for the strains measured at the distal palmar strain gage was 1045 ± 634 με/day, at the distal dorsal thumb side strain gage was 3240 ± 1842 με/day, and at the distal dorsal ulna side strain gage was 4615 ± 1634 με/day. The DSS for the entire ultra-distal region containing the strain gages was 4027 ± 1566 με/day.

3.4 Discussion

Non-invasive subject-specific finite element methods to quantify bone strain are necessary to accurately understand the mechanical environment experienced by the bone. The objective of this study was to create and validate methods for subject specific finite element model generation to predict the surface strains experienced by the distal radius during a specific

loading activity. The model generation methods were validated by comparing the experimentally measured strains with the strains predicted by the model.

To determine the element size to be used for modeling the radius, convergence analysis were performed. The convergence response could vary based on the specimen selected for analysis. Therefore, all available specimens were used to obtain an average converged element size. In this study, tetrahedral elements with a nominal volume of 0.5 mm^3 were based on the analysis. Linear elastic and hyperelastic cartilage material properties were tested here. The average maximum and minimum principal strains at a 5 mm section at the ultra-distal radius were not sensitive to the cartilage material properties tested here, with the average coefficient of variance over all specimens being 4% for maximum principal strain, and 2.3% for minimum principal strain. Hyperelastic material property was selected for further analysis since it most accurately describes cartilage material behavior, and is widely used in FE models (Anderson DD, 2005; Edwards, 2012).

Of the four density-elasticity relations analyzed, the models developed using Eq. (iv) (Morgan, 2003) predicted principal strains that were most accurately matched with the principal strains measured experimentally, with r = 0.928, and a slope of 0.809. One of the four specimens was suspected to be highly osteoarthritic, the carpal bones were observed to be partially fused to the radius and ulna. The magnitudes of maximum principal strains for this specimen were over-predicted by an average of 418 με, and the magnitudes of minimum principal strains were over-predicted by an average 432 με by the FE model. For the three other specimens, predicted maximum principal strains were 21 με, 100 με, and -34 με different from the respective measured strains, and predicted minimum principal strains were 54 με, -45 με, and 199 με different from the corresponding measured strain. Osteoarthritis causes calcification within the

joint, which results in lower joint mobility. The discrepancy between predicted and measured strain suggests that the osteoarthritic condition may have resulted in more force being transferred through the ulna. Exclusion of this specimen from the analysis resulted in a more accurate relation between predicted and measured strains, with r = 0.968, and a slope of 0.984 that was not significantly different from 1, as well as lower measured errors.

Other similar *in-vitro* FE validation studies have shown reasonable accuracies, with r=0.769, standard error (S.E.) = 311 με (Keyak, 1993), r = 0.91, RMSE = 8.9% (Taddei, 2006), r = 0.898, S.E. = 102 με (Gupta, 2004), r = 0.91 (Anderson AE, 2005), and r = 0.954, RMSE = 9.8% (Schileo, 2007). The large range of accuracies can be explained by several factors such as density-elasticity equation, location tested, number of specimens, loading conditions, and model meshing technique. For example, these studies focused on the femur, scapula, and pelvis, used 1-4 specimens, used voxel and geometry based meshing techniques, and were used to predict strains and fracture load. The results from this study can be compared with a similar subject specific FE model validation of the human distal radius from our group, where periosteal surface strains were accurately predicted with r = 0.9 and RMSE = 13.4% (Edwards, 2012). That validation study tested three out of the four constitutive equations, the same location, and a similar number of specimens compared to this study. The previous validation study used Eq (i) in the validated models, compared to Eq (iv) in this study. This disparity may be explained by three major differences between the studies. A bone reconstruction kernel was used on the CT data in the Edwards et. al validation study compared to a standard reconstruction kernel used here. A comparison of bone and standard reconstruction kernels for a sample subset of subjects showed that the density values obtained from the bone reconstruction kernel were 4.5% higher than those obtained from the standard reconstruction. The bone reconstruction also had a 16% higher

standard deviation than that of standard reconstruction. The previous validation study assigned median density values of the enclosed voxels to the corresponding elements compared to the mean values of the enclosed voxels in this study. These two factors may result in the bone being assigned stiffer material properties in that study when compared to the current study. Additionally, the current study uses quadratic tetrahedral elements compared to linear hexahedral elements in the previous study, and may influence the results.

The Daily Strain Stimulus provides an estimate of the mechanical stimulus experienced by the bone on account of the loading task, and has been related to bone adaptation in animal models (Chen, 2010; Adams, 1997). Mikic et al. used *in-vivo* strain gage data (Lanyon, 1975) to calculate the daily strain stimulus at the human antero-medial tibia during walking and jogging activities. The DSS values varied between 1389 με/day to 4836 με/day for the individual activities, and 4900 με/day for all activities combined. These values were calculated for based on 1000 cycles per activity. The DSS for the loading activity used here was calculated for 50 cycles and was based on our *in-vivo* loading protocol (Troy, 2013), and is comparable to that study. The DSS can be similarly calculated using the predicted strains from the FE model validated here and along with a prospective study could be used to directly relate bone adaptation with applied stimulus in humans.

This study is limited by the use of a small sample size. However, as mentioned above many specimen-specific finite-element model validation studies have relied on sample sizes similar to that used in this study. Additionally, the density-elasticity relationships examined herein were derived from anatomical locations other than the distal radius. However, we are unaware of a density-elasticity relationship specific to the distal radius. Given these limitations, we were able to validate a modeling method that can accurately (r=0.968, RMSE=11.1%) and

non-invasively predict periosteal strains acting on the radius bone during a targeted loading task of leaning on to the palm of the hand. The validated model can be used to assess exercise-induced bone strain to better understand the mechanical factors contributing to bone adaptation in humans.

Chapter 4. Aim 2

Aim 2a: Determine whether the prescribed exercise regime is osteogenic by comparing whole bone BMC and fracture strength at baseline and after the exercise regime.

Aim 2b: Determine whether change in BMC is more closely related to force magnitude or strain magnitude by comparing a fixed force exercise group to a fixed strain exercise group.

4.1 Introduction

Bone adapts its form and function, and this adaptation is driven by the mechanical stimulus experienced by the bone. Net bone apposition occurs when the applied mechanical stimulus exceeds a maximum homeostatic threshold, while net bone resorption occurs when the applied mechanical stimulus falls below a minimum homeostatic threshold. This ability of bone to adapt to mechanical stimuli has allowed exercise-based interventions to be considered as a practical option to prevent bone loss and enhance bone strength.

Animal models have been valuable tools for understanding the process of bone adaptation, and have been studied with the long term goal of developing mechanical loading-based interventions to improve bone strength in humans. Using these animal models, the magnitude of the adaptive response has been attributed to the characteristics of the mechanical stimulus such as strain, strain rate, and number of loading cycles (Rubin, 1985; Rubin, 1984; O'Connor, 1982; Srinivasan, 2002). Since bone is fundamentally similar between species, these factors would be expected to also apply to bone adaptation in humans; however, the specific manner in which these factors affect human bone may be different.

Our purpose was to develop and examine an *in-vivo* loading model to study the interaction between mechanical loading and bone adaptation in humans. The mechanical loading protocol used here was designed to directly translate results from the rat ulna loading model (Torrance, 1994) to the human distal radius. In humans, upper extremities experience less habitual loads than lower extremities, thus may be more responsive to voluntarily applied physiologically relevant loads beyond those experienced during activities of daily living. The distal radius is a common site of fracture as a consequence of falls in older adults, and strengthening this site could reduce fracture risk. Additionally, distal radius is easily imaged non-invasively with low-risk, and an exercise task targeting the distal radius is easy to implement and manipulate. Our hypothesis was that the loading protocol would result in a mechanical stimulus above the homeostasis threshold at the distal radius, leading to an osteogenic response over time. Additionally, we expected this response to be more directly related to strain magnitude rather than the force magnitude of the applied stimulus.

4.2 Methods

4.2.1 Subjects

Thirty-nine healthy women (27 experimental, 12 control) ages 21-35 with a BMD t-score greater than -2.5, a normal BMI (18.5-25), and regular menstrual activity were recruited for this study. All methods were approved by the Institutional Review Board at the University of Illinois at Chicago and all subjects provided written informed consent prior to their participation. This study focused on women due to their high rate of fragility fractures later in life. Women in this age group are known to have attained peak BMC (Henry, 2004), and are not affected by

menopause, therefore any observed changes would be expected to result from the loading protocol.

4.2.2 Mechanical Loading Protocol

Subjects were instructed to voluntarily apply an axially-directed force to the wrist by leaning onto the palm of their non-dominant hand. The non-dominant radius was chosen based on the expectation that it would be more responsive to the novel loading protocol, based on the assumption that it experiences less habitual mechanical loading than the dominant radius. Subjects applied the force 50 cycles per day, 3 days per week, for 28 weeks, with each cycle being separated by 2 seconds. A portable voice recorder provided sound cues to assist the subjects in loading at the correct time interval. The subjects applied the force on a scale or load cell to provide real-time visual feedback of force magnitude, in the form of i) analog scale reading, ii) digital force waveform, or iii) light indicators. The 27 experimental subjects were assigned a target of either 1) a fixed force of 300N (13 subjects), or 2) a force that was expected to produce a periosteal surface strain of 1100με at the distal radius (14 subjects), based on the subject's individual anatomy, preliminary data and a previously validated FE model. Twelve additional subjects were assigned to the control group. Based on power analysis of preliminary data, a sample size of 10 subjects per group was found to be sufficient to detect a 40 mg change (corresponding to a change of 1%) in total BMC at the distal radius (90% power, α=0.05) over 28 weeks of loading.

4.2.3 CT Data Collection and Registration

Clinical CT data were collected on the loaded arm of all subjects at weeks 0, 14 and 28. Images were acquired on a single clinical scanner (GE Brightspeed, GE Medical, Milwaukee,

WI) with settings of 120 kV, 180 mA and a voxel size of 234 x 234 x 625 μm. Each CT scan included a calibration phantom (QRM, Moehrendorf, Gemany) to convert CT attenuation in Hounsfield unit (HU) to hydroxyapatite density (ρ_{ha}). The native images of the baseline scans were manually aligned along the long axis of the radius using Mimics v14.0 (Materialise, Leuven, Belgium). The periosteal surface of the radius was segmented from the scans using a density threshold of 0.175 g/cm^3. Successive scans were registered to the corresponding segmented baseline scans for all subjects (Figure 4-1) using ICP-FINITE (Matlab Central File Exchange), which is an iterative closest point registration algorithm for 3D point clouds, available through Matlab Central File Exchange. A precision study demonstrated the mean absolute error for this registration procedure in our laboratory to be 0.00±0.00°, 0.00±0.00°, and 0.7±0.7° for rotations about the AP, ML, and longitudinal axis of the radius. The CT data were used to quantify changes to bone mass, structure and strength, and as the basis for subject-specific finite element models.

4.2.4 QCT Analysis

The CT scan data were analyzed following image registration to the baseline scans. An ultra-distal, mid-cortical and a total radius region were selected for analysis (Figure 4-2). The ultra-distal region was defined as the 9.375 mm region proximal to the subchondral plate and corresponds to the region typically selected for analysis in high resolution peripheral quantitative CT images (HR-pQCT) (Hansen, 2010). The mid-cortical region was defined as a 45 mm region proximal to the subchondral plate, excluding the ultra-distal region. The total radius was defined as the 45 mm region proximal to the subchondral plate, as well as everything distal to and including the subchondral plate. The location of the subchondral plate was objectively defined for the first scan (week 0) as the transverse CT slice with the largest cross-sectional area. This

location was standardized relative to the distal-most transverse slice of the radius for subsequent scans (weeks 14 and 28) to ensure the same region was being compared between time points. For each region, bone volume (BV; cm^3), volumetric bone mineral density (vBMD; g/cm^3) and bone mineral content (BMC; g) were calculated for integral, cortical, and trabecular regions of bone (Figure 4-3). The integral region included all voxels contained within the periosteal surface boundary. All voxels with a hydroxyapetite equivalent density greater than or equal to 0.335 g/cm^3 were considered cortical bone, while voxels with a density lower than this were considered trabecular bone (including the associated marrow space). This density cut-off represented the average value that best visually defined the cortical shell in a subset of 15 individual CT scans, and agreed well with values from published literature (Marshall, 2006). Additionally, cross-sectional area (CSA; cm^2), compressive strength index (CSI; g^2/cm^4), and bending strength index (BSI; cm^3) were calculated and averaged for both the ultra-distal and mid-cortical regions.

$CSI = CSA \times iBMD^2$

$BSI = \frac{I_x+I_y}{W}$, (I_x+I_y) is the polar moment of inertia, W is the effective bone diameter,

$$W = 2\sqrt{\frac{CSA}{\pi}}$$

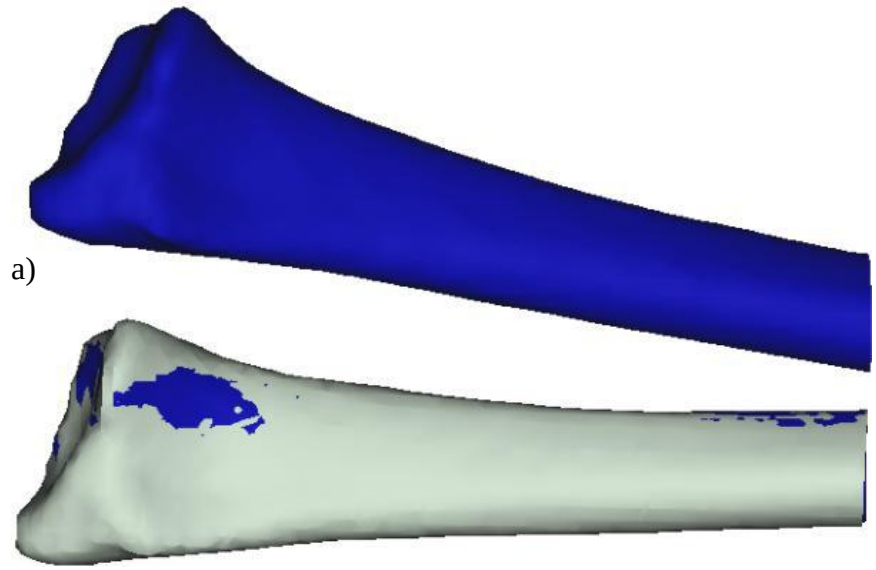

a)

b)

Figure 4-1: a) Segmented CT scan and b) registered into baseline segmented CT scan.

Strength measures CSI and BSI are functions of both mineral density and structure, and have previously been used as measures of bone adaptation (Lang, 2004). All parameters measured here are shown in Table 4-1. Repeatability error for these segmentation, registration, and analysis methods have been found to be less than 0.72% for bone mineral parameters and less than 0.97% for bone strength parameters (Bhatia, 2012).

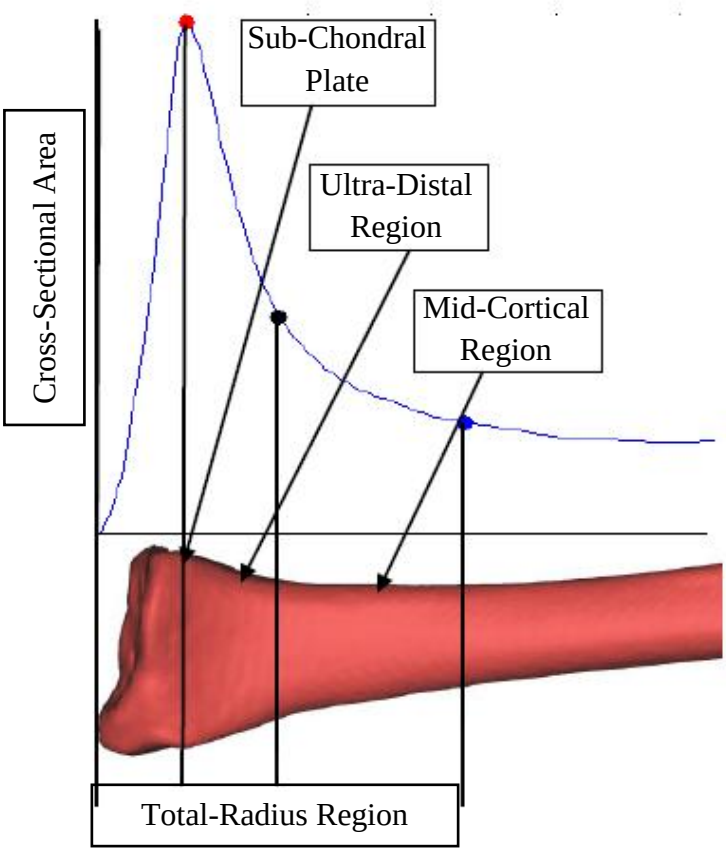

Figure 4-2: Identification of subchondral plate, Ultra-distal region, Mid-cortical region, and the Total-radius region.

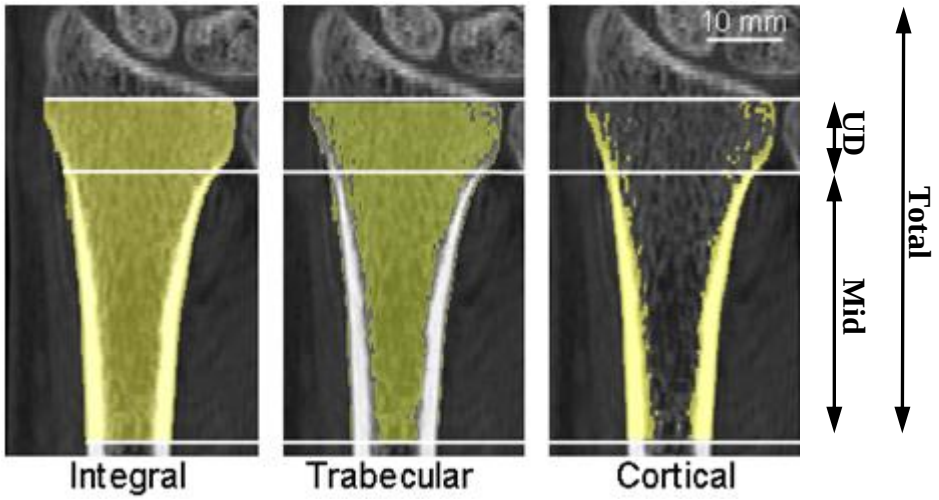

Figure 4-3: Definition of QCT analysis regions.

4.2.5 Compliance and Force Data Collection

All subjects in the loading groups were instructed to fill out a loading log-sheet to record compliance. Additionally, the subjects were asked to digitally record at least one loading session a week in our laboratory (Figure 4-4a). A subset of the subjects were given portable loading devices to take home (Figure 4-4b). Both these methods allowed for recording of the actual force applied (Figure 4-4c). The portable loading device consisted of a load cell, a stand-alone data-logger, and gave real time feedback using LED lights by comparing applied force with assigned force. The portable loading device allowed for the measurement of the actual compliance in addition to self-reported compliance. Subjects with compliance of less than 50% after 28 weeks were considered as non-compliant.

a) 

b) 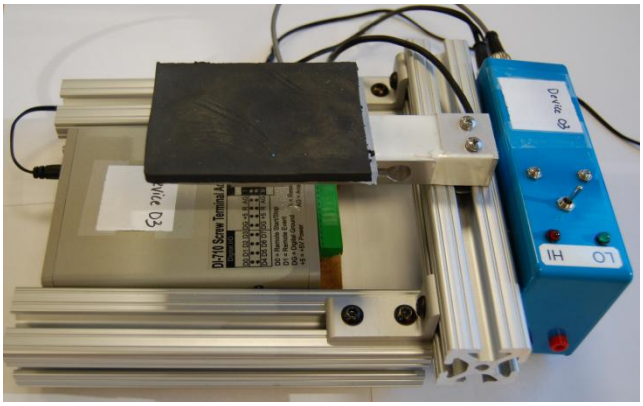

c) 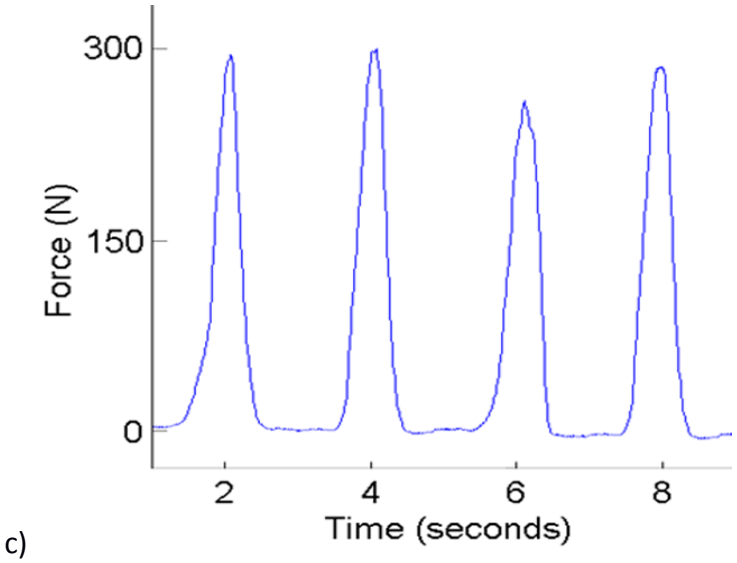

Figure 4-4: a) Load cell for laboratory loading session, b) portable loading device, c) sample recording of applied force

4.2.6 In-vivo Strains

The segmented and aligned baseline scans were used to build finite element models using previously validated procedures (see Chapter 3). For each subject, models were run using boundary conditions corresponding to this loading task, and mean and maximum effective strains

were calculated at the surface as well as the entire section corresponding to the UD region (Figure 4-5).

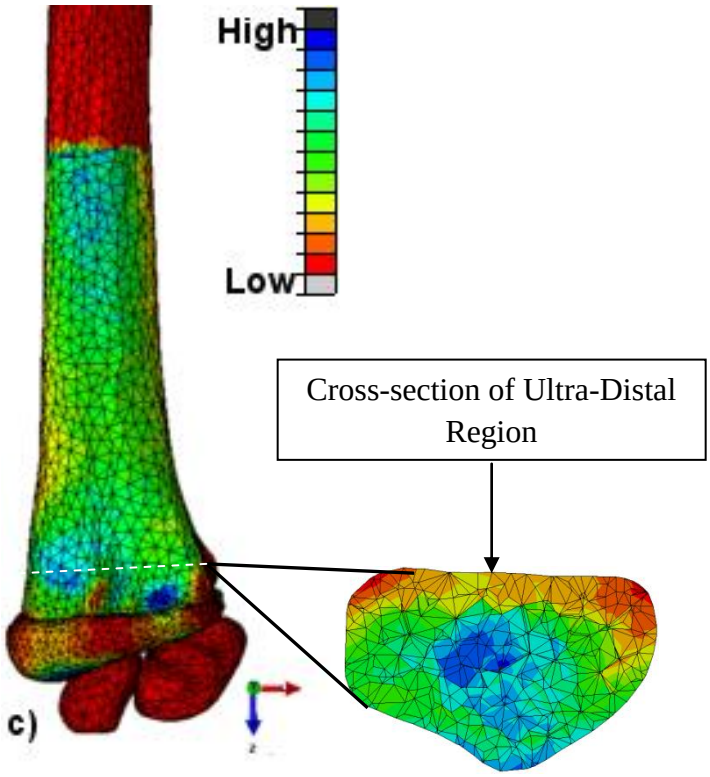

Figure 4-5: Finite element minimum principal strain map under the applied loading protocol.

Table 4-1: Bone mineral and strength parameters

Parameter		Units
Ultra-Distal Integral Bone Volume	UDiBV	
Ultra-Distal Trabecular Bone Volume	UDtBV	
Ultra-Distal Cortical Bone Volume	UDcBV	
Mid-Cortical Integral Bone Volume	MidiBV	
Mid-Cortical Trabecular Bone Volume	MidtBV	cm^3
Mid-Cortical Cortical Bone Volume	MidcBV	
Total Integral Bone Volume	TotiBV	
Total Trabecular Bone Volume	TottBV	
Total Cortical Bone Volume	TotcBV	
Ultra-Distal Integral Bone Mineral Content	UDiBMC	
Ultra-Distal Trabecular Bone Mineral Content	UDtBMC	
Ultra-Distal Cortical Bone Mineral Content	UDcBMC	
Mid-Cortical Integral Bone Mineral Content	MidiBMC	
Mid-Cortical Trabecular Bone Mineral Content	MidtBMC	g
Mid-Cortical Cortical Bone Mineral Content	MidcBMC	
Total Integral Bone Mineral Content	TotiBMC	
Total Trabecular Bone Mineral Content	TottBMC	
Total Cortical Bone Mineral Content	TotcBMC	
Ultra-Distal Integral Bone Mineral Density	UDiBMD	
Ultra-Distal Trabecular Bone Mineral Density	UDtBMD	
Ultra-Distal Cortical Bone Mineral Density	UDcBMD	
Mid-Cortical Integral Bone Mineral Density	MiBMD	
Mid-Cortical Trabecular Bone Mineral Density	MidtBMD	g/cm^3
Mid-Cortical Cortical Bone Mineral Density	MidcBMD	
Total Integral Bone Mineral Density	TotiBMD	
Total Trabecular Bone Mineral Density	TottBMD	
Total Cortical Bone Mineral Density	TotcBMD	
Ultra-Distal Cross Sectional Area	UDCSA	cm^2
Mid-Cortical Cross Sectional Area	MidCSA	
Ultra-Distal Compressive Strength Index	UDCSI	g^2/cm^4
Mid-Cortical Compressive Strength Index	MidCSI	
Ultra-Distal Bone Strength Index	UDBSI	cm^3
Mid-Cortical Bone Strength Index	MidBSI	

4.2.7 Data Analysis

To test the hypothesis that the loading protocol is osteogenic, repeated measures ANOVAs were used to examine time related changes in bone parameters in each group. Baseline, 14 week, and 28 week were the three time points, and exercise and control were the two groups. For the parameters in which a significant main effect of time was found, post-hoc paired t-tests with Bonferroni corrections were performed. To compare between groups, independent t-tests were performed on the change in each parameter versus baseline at 14 and 28 week time points. Means, standard deviation and inter-quartile range (iqr) was calculated for applied force and strain magnitudes for the subjects of the fixed strain and fixed force groups. To test the hypothesis that the osteogenic response is more directly related to the strain magnitude and not the force magnitude of the applied stimulus, Pearson's r correlations were calculated for the percent change in these parameters over 14- and 28- weeks versus strain for the fixed force group, and versus force for the fixed strain group. Subject compliance was defined as the percent of total assigned bouts completed. An independent two-sample t-test was performed to compare subject compliance between time points. SPSS v.12.0 (SPSS, Chicago, IL) was used for all statistical calculations and an alpha criterion of 0.05 was set.

4.3 Results

Thirty-three out of thirty-seven subjects completed 14 weeks or more of the study, and twenty-eight of those completed all 28 weeks of the study. Four subjects dropped out of the study before completion of 14 weeks, or were excluded due to non-compliance of experimental conditions, and are not reported here. Five subjects dropped out between 14 and 28 week time points, and their 28 week data points were imputed based on the 14 to 28 week response of the other subjects in the corresponding groups. Subjects were significantly more compliant in the

first 14 weeks of the study compared to the last 14 weeks, with the average self-reported compliance being 81.54% in the first 14 weeks and 54.41% between 14 and 28 weeks (p=0.015). The subjects in the fixed strain group applied an average force of 371.4 ± 36 N (iqr = 52.7 N), corresponding to a mean distal equivalent surface strain of 430 ± 159 με (iqr = 151 με) whereas the subjects in the fixed force group applied an average force of 333.3 ± 28 N (iqr = 42.7 N), corresponding to a mean distal equivalent surface strain of 478 ± 159 με (iqr = 259 με). The mean and standard deviations for mineral and strength parameters at the three time points for the control and combined experimental groups are shown in Table 4-2.

Over the 28 week loading protocol, at the ultra-distal radius a significant effect of time was observed in the integral and trabecular BMD for the control group, and in the integral BMD, and trabecular BV, BMC and BMD for the exercise group. At the mid-cortical region, there was a significant effect of time in integral BMC, trabecular BMD, and cortical BV and BMC for the control group, and no effect of time was observed in the exercise group. For the total-radius region, a significant effect of time was observed in integral BMC and BMD, trabecular BMD, and cortical BV and BMC for the control group, and in integral BV, and trabecular BV and BMC for the exercise group. A significant effect of time was observed in UDCSI and MidCSI for the control group, and in UDCSI for the exercise group. At each of these locations, there was a general decreasing trend in the parameters in the control group, and a general increasing trend or no change in the exercise group (Table 4-2).

Table 4-2: Means and standard deviations for control and exercise groups for all time points. * $p<0.05$ between 28 week and baseline values, † $p<0.05$ between 14 week and baseline values, ‡ $p<0.05$ between 28 week and 14 week values. All p values are Bonferroni corrected.

	Control Group					
	Baseline (n=12)		14 Weeks (n=12)		28 Weeks (n=12)	
	Mean	SD	Mean	SD	Mean	SD
UDiBV	3.991	0.374	4.018	0.366	3.996	0.378
UDiBMC	0.977	0.152	0.964	0.156	0.960	0.153
UDiBMD *	0.246	0.040	0.241	0.042	0.241	0.040
UDtBV	3.142	0.448	3.199	0.472	3.185	0.460
UDtBMC	0.570	0.088	0.572	0.090	0.570	0.088
UDtBMD	0.184	0.033	0.181	0.034	0.181	0.032
UDcBV	0.849	0.228	0.820	0.252	0.812	0.237
UDcBMC	0.407	0.121	0.393	0.130	0.390	0.125
UDcBMD	0.476	0.028	0.476	0.024	0.477	0.027
MidiBV	6.806	0.884	6.835	0.844	6.791	0.881
MidiBMC *	3.603	0.454	3.575	0.443	3.559	0.437
MidiBMD	0.533	0.059	0.526	0.058	0.528	0.058
MidtBV	2.975	0.710	3.035	0.684	3.002	0.709
MidtBMC	0.452	0.112	0.452	0.110	0.448	0.109
MidtBMD †	0.155	0.038	0.152	0.039	0.152	0.037
MidcBV	3.832	0.456	3.800	0.432	3.790	0.427
MidcBMC *	3.151	0.404	3.124	0.387	3.111	0.389
MidcBMD	0.822	0.036	0.822	0.032	0.821	0.036
TotiBV *	13.936	1.487	13.981	1.404	13.874	1.496
TotiBMC *	5.623	0.706	5.565	0.688	5.539	0.693
TotiBMD *	0.405	0.040	0.399	0.041	0.400	0.039
TottBV	8.021	1.302	8.154	1.308	8.064	1.286
TottBMC	1.437	0.224	1.436	0.218	1.424	0.216
TottBMD * †	0.181	0.029	0.178	0.030	0.178	0.028
TotcBV	5.915	0.851	5.826	0.829	5.810	0.825
TotcBMC *	4.186	0.601	4.129	0.582	4.115	0.581
TotcBMD	0.708	0.027	0.709	0.025	0.709	0.028
UDCSA	4.311	0.397	4.340	0.389	4.315	0.402
MidCSA	1.911	0.248	1.919	0.237	1.906	0.247
UDCSI *	0.264	0.086	0.257	0.089	0.255	0.086
MidCSI *	0.542	0.112	0.531	0.110	0.530	0.108
UDBSI	0.065	0.015	0.064	0.015	0.064	0.015
MidBSI	0.135	0.026	0.134	0.026	0.133	0.025

	Exercise Group					
	Baseline (n=23)		14 Weeks (n=23)		28 Weeks (n=23)	
	Mean	SD	Mean	SD	Mean	SD
UDiBV	3.781	0.406	3.805	0.410	3.806	0.402
UDiBMC	0.978	0.258	0.986	0.256	0.975	0.260
UDiBMD ‡	0.257	0.051	0.258	0.049	0.255	0.050
UDtBV *	2.838	0.396	2.858	0.391	2.879	0.389
UDtBMC * †	0.519	0.071	0.527	0.070	0.526	0.069
UDtBMD	0.185	0.032	0.187	0.031	0.185	0.031
UDcBV	0.943	0.428	0.947	0.446	0.927	0.454
UDcBMC	0.460	0.234	0.459	0.236	0.449	0.237
UDcBMD	0.479	0.033	0.477	0.036	0.477	0.034
MidiBV	6.363	0.847	6.384	0.850	6.382	0.840
MidiBMC	3.383	0.530	3.385	0.522	3.380	0.510
MidiBMD	0.534	0.066	0.533	0.064	0.532	0.064
MidtBV	2.746	0.652	2.761	0.651	2.758	0.642
MidtBMC	0.405	0.078	0.409	0.081	0.410	0.079
MidtBMD	0.153	0.039	0.154	0.039	0.154	0.038
MidcBV	3.617	0.472	3.623	0.473	3.624	0.473
MidcBMC	2.978	0.488	2.975	0.480	2.971	0.466
MidcBMD	0.821	0.034	0.819	0.036	0.818	0.032
TotiBV	12.848	1.580	12.889	1.585	12.887	1.574
TotiBMC	5.346	0.983	5.354	0.959	5.329	0.938
TotiBMD	0.416	0.050	0.415	0.048	0.414	0.049
TottBV *	6.996	1.188	7.021	1.158	7.065	1.182
TottBMC *	1.243	0.147	1.256	0.147	1.260	0.145
TottBMD	0.181	0.030	0.182	0.030	0.182	0.030
TotcBV	5.852	1.277	5.867	1.261	5.823	1.254
TotcBMC	4.103	0.917	4.099	0.893	4.070	0.872
TotcBMD	0.701	0.020	0.698	0.023	0.699	0.022
UDCSA	4.085	0.437	4.110	0.440	4.110	0.432
MidCSA	1.786	0.238	1.792	0.239	1.791	0.236
UDCSI ‡	0.285	0.142	0.286	0.138	0.280	0.139
MidCSI	0.513	0.137	0.511	0.131	0.510	0.128
UDBSI	0.068	0.028	0.068	0.027	0.067	0.026
MidBSI	0.122	0.032	0.122	0.031	0.121	0.030

At the ultra-distal region, changes in integral BMC, BMD, and trabecular BMD were significantly different after 14 weeks, and changes in trabecular BMD were significantly different between groups after 28 weeks. At the mid-cortical region, changes in trabecular BMD and cortical BV were significantly different between groups after 14 weeks, and changes in integral BMC, trabecular BMD, and cortical BV and BMC were significantly different between groups after 28 weeks. At the total radius regions, changes in integral BMD, trabecular BMD, and cortical BV were significantly different between groups after 14 weeks, and changes in integral BV and BMC, and trabecular BMC and BMD were significantly different between groups after 28 weeks. Changes in MidCSI were significantly different between groups after 14 and 28 weeks, and changes in UDCSI were significantly different between groups after 14 weeks. In each of the above reported parameters, a consistent decrease was observed over time in the control group, whereas for the exercise group an increase, or a decrease smaller than the ones observed in the control group were observed.

For the fixed strain group, no significant correlations were observed between applied-force and percent change in any mineral or strength parameters. However, for the fixed force group, positive and moderately strong significant correlations were observed between the mean measures of applied strain and percent change in UDiBV, UDiBMC, UDtBMC, UDtBMD, UDCSA, MidCSA, and UDCSI in the first 14 weeks (Table 4-3). Plots for percent change in selected mineral and strength parameters versus applied strain and versus applied force are shown in Figure 4-6.

Table 4-3: Pearson's r correlations between applied Force and applied Strains, and percent change in bone mineral and strength parameters after 14 weeks of the loading protocol. Values in bold are significant correlations ($p<0.05$)

Fixed Force Correlations						Fixed Strain Correlations	
Energy Equivalent Strains	Mean Distal Surface	Max Distal Surface	Mean Distal Whole	Max Distal Whole			Applied Force
UDiBV	**0.743**	0.539	**0.732**	**0.661**		UDiBV	0.356
UDiBMC	**0.775**	**0.685**	**0.764**	**0.789**		UDiBMC	0.243
UDiBMD	0.383	0.435	0.378	0.470		UDiBMD	-0.073
UDtBV	0.545	0.278	0.529	0.391		UDtBV	0.193
UDtBMC	**0.772**	0.485	**0.754**	**0.624**		UDtBMC	0.239
UDtBMD	**0.707**	0.545	**0.695**	**0.648**		UDtBMD	0.148
UDcBV	0.298	0.555	0.282	0.477		UDcBV	0.316
UDcBMC	0.220	0.468	0.203	0.380		UDcBMC	0.147
UDcBMD	-0.136	0.016	-0.146	-0.083		UDcBMD	-0.443
MidiBV	**0.609**	0.402	**0.603**	0.529		MidiBV	0.371
MidiBMC	0.444	0.298	0.518	0.410		MidiBMC	-0.053
MidiBMD	-0.336	-0.221	-0.275	-0.275		MidiBMD	-0.288
MidtBV	0.586	0.394	0.558	0.489		MidtBV	0.321
MidtBMC	**0.603**	0.350	0.586	0.513		MidtBMC	0.151
MidtBMD	0.494	0.164	0.511	0.448		MidtBMD	-0.301
MidcBV	-0.063	-0.066	0.028	-0.011		MidcBV	0.314
MidcBMC	0.010	0.036	0.088	0.014		MidcBMC	-0.093
MidcBMD	0.045	0.078	0.087	0.023		MidcBMD	-0.338
TotiBV	-0.337	-0.282	-0.327	-0.347		TotiBV	0.489
TotiBMC	0.212	0.194	0.267	0.218		TotiBMC	0.043
TotiBMD	0.406	0.356	0.449	0.419		TotiBMD	-0.135
TottBV	-0.096	-0.170	-0.127	-0.207		TottBV	0.263
TottBMC	0.152	-0.031	0.125	0.031		TottBMC	0.179
TottBMD	0.435	0.198	0.429	0.370		TottBMD	-0.084
TotcBV	-0.216	-0.011	-0.148	-0.036		TotcBV	0.267
TotcBMC	0.091	0.185	0.152	0.147		TotcBMC	0.037
TotcBMD	0.378	0.289	0.394	0.260		TotcBMD	-0.443
UDCSA	**0.742**	0.537	**0.731**	**0.658**		UDCSA	0.359
MidCSA	**0.609**	0.402	**0.603**	0.529		MidCSA	0.371
UDCSI	**0.628**	**0.605**	**0.618**	**0.678**		UDCSI	0.078
MidCSI	-0.011	-0.004	0.072	0.015		MidCSI	-0.202
UDBSI	0.243	0.301	0.251	0.274		UDBSI	0.061
MidBSI	0.456	0.371	0.498	0.392		MidBSI	-0.150

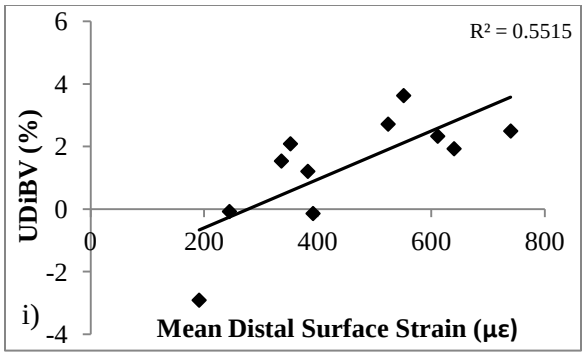
R² = 0.5515
UDiBV (%)
Mean Distal Surface Strain (με)
i)

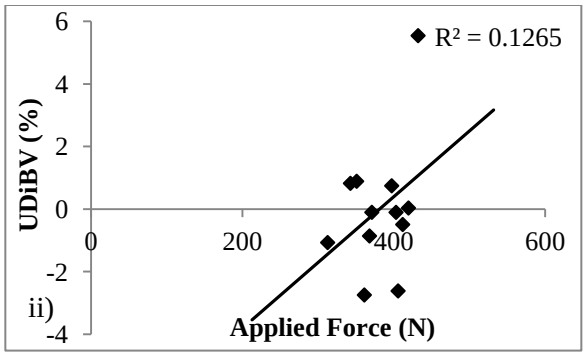
R² = 0.1265
UDiBV (%)
Applied Force (N)
ii)

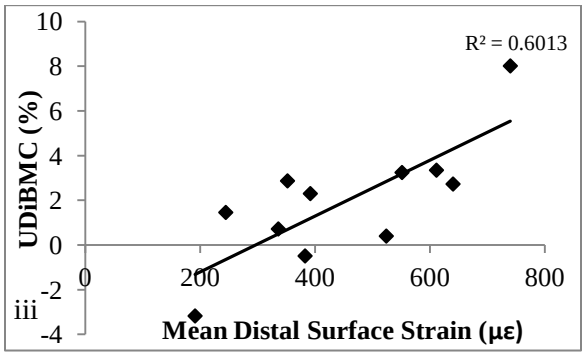
R² = 0.6013
UDiBMC (%)
Mean Distal Surface Strain (με)
iii

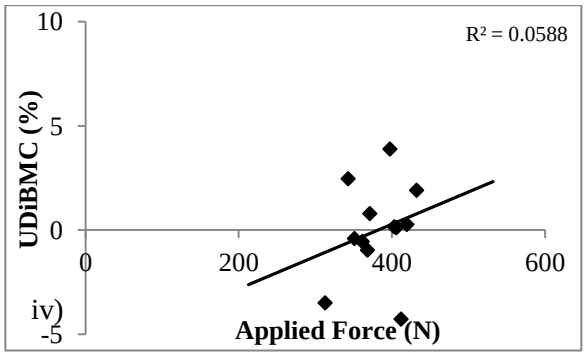
R² = 0.0588
UDiBMC (%)
Applied Force (N)
iv)

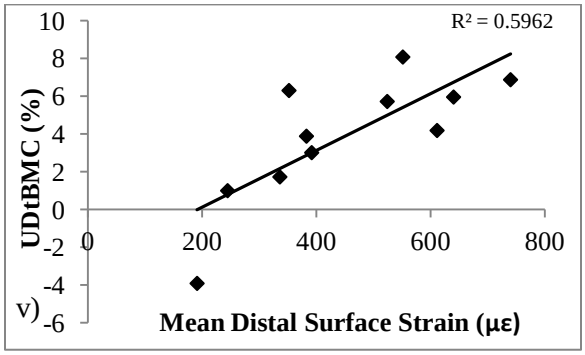
R² = 0.5962
UDtBMC (%)
Mean Distal Surface Strain (με)
v)

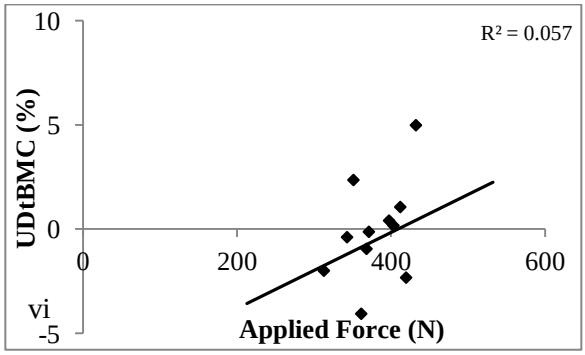
R² = 0.057
UDtBMC (%)
Applied Force (N)
vi

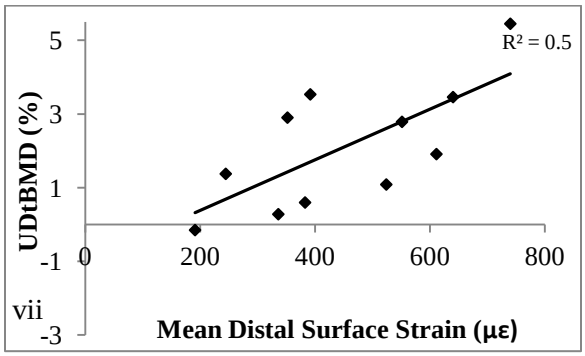
R² = 0.5
UDtBMD (%)
Mean Distal Surface Strain (με)
vii

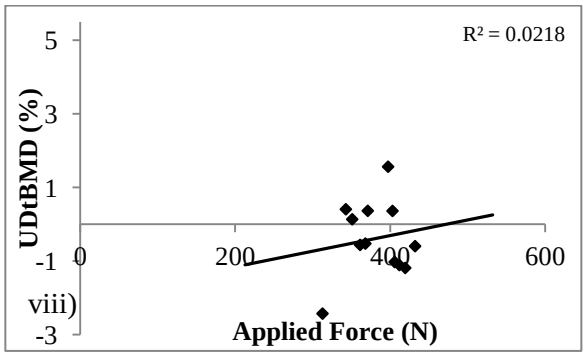
R² = 0.0218
UDtBMD (%)
Applied Force (N)
viii)

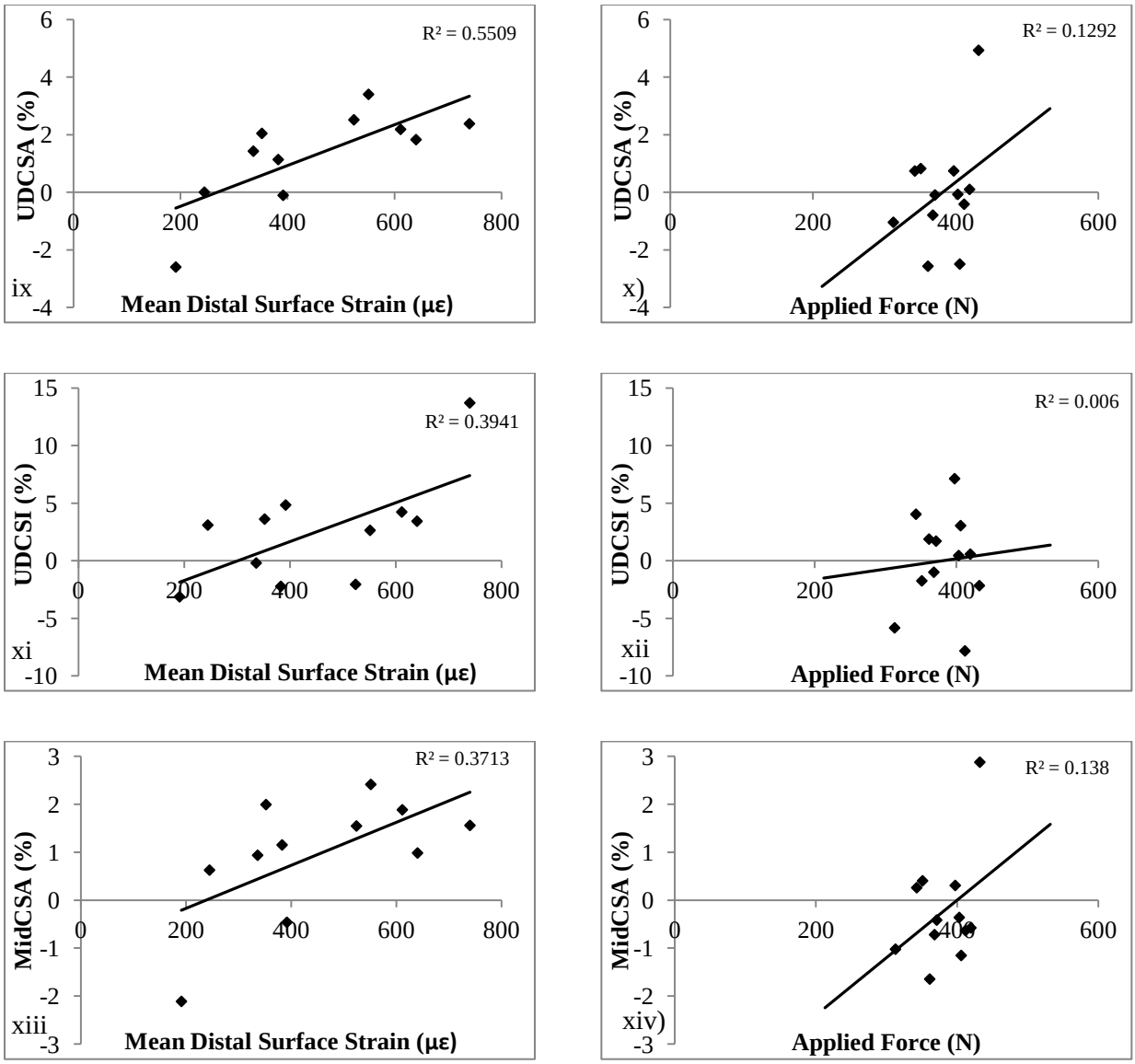

Figure 4-6: Scatter plots of percent change in selected mineral and strength parameters versus mean distal surface strain and applied force

4.4 Discussion

Our aim was to quantify the degree to which our novel *in*-vivo loading protocol resulted in an osteogenic response. In general, a small but significant decrease in many mineral and strength parameters were observed over time in the subjects of the control group. Small significant increases or no changes were observed in the same period of time in the exercise groups. Our results have shown that the loading task of leaning onto the palm of the hand resulted in a mechanical stimulus that was osteogenic in adult women. Additionally, the hypothesis that the osteogenic response is more directly related to the strain magnitude than force magnitude of the applied stimulus was supported.

The ultra-distal radius of women reaches peak BMC at age 23 and achieves 94% of peak BMC by age 16, as measured by DXA (Henry, 2004). Others have reported no age-related differences in ultra-distal BMC in women age 15-17 versus 18-21 when measured using HR-pQCT (Kirmani, 2009). Although we cannot discount the possibility that the observed changes in BMC and other variables may have occurred as a result of subject aging, we note that in contrast to experimental subjects, the control subjects experienced a decrease in most measures, and these subjects were of similar age to the experimental subjects. The subjects selected for this study were healthy young women, hence osteoporosis, or hormonal imbalance were unlikely reasons for the observed changes. The decrease in the control subjects instead may be attributed to seasonal changes. Indeed, bone density has been previously observed to show a seasonal variation of 0.3% - 4.5% over a year with a maximum bone density observed in the months of summer and a minimum in the months of winter (Bergstralh, 1990; Rapuri 2002; Meier, 2004; Viljakainen, 2006), and may be associated with seasonal variance in physical activity, dietary intake, and sun exposure (Pasco, 2002; Meier, 2004). Since the baseline scans for all subjects,

both in the exercise and the control groups, were obtained around the same time of the year, between August and October, it can be said that the loading task prevented the seasonal decrease in bone parameters, and was osteogenic to some degree.

On further analyses of changes over time, largest increases in mineral and strength parameters were observed in the first 14 weeks of the study for the subjects in the exercise groups, smaller increases, or decreases in these parameters were observed between 14 and 28 weeks for these subjects (Table 4-2). This can be attributed to our observation that on an average, subjects were significantly more compliant in the first 14 weeks of the study than the last 14 weeks. Others have reported this decrease in adherence over the course of exercise interventions, with adherence dropping from 80% in the first 8 weeks, to 45% at 16 weeks, and 39% at 26 weeks (Lynch, 1992), and positively associated with the perceived seriousness of the issue, and expected benefits of the intervention.

Significant increases in UDtBV, UDtBMC, TotiBV, TottBV, and TottBMC were observed for the exercise group. Since TotiBV includes the cortical bone, trabecular bone, as well as the marrow space, the increase in TotiBV can be attributed to detection of additional voxels on the periosteal surface. No changes were observed in the mid-cortical region, suggesting periosteal bone formation at the ultra-distal region and the region distal to the sub-chondral plate. The applied stimulus was mostly in axial compression, with the ultra-distal radius being the region the force was directly transmitted to through the palm of the hand and experienced larger strains compared to the more proximal regions (Troy, 2013). Additionally, a quicker adaptation response is expected due to the larger surface area of the trabecular bone, as well as abundance of mesenchymal stem cells due to the proximity to the marrow space. For the control group, decreases in integral and trabecular BMD were observed in the ultra-distal, mid-

cortical, and total-radius regions in the first 14 weeks. Additionally, although not significant, increases in trabecular BV and decreases in cortical BV were observed in these three regions, suggesting endocortical resorption.

The changes observed in both the control and exercise groups may be affected by the limitations of threshold-based methods of classifying cortical and trabecular bone. Some voxels initially classified as one could be reclassified as the other indicating cortical thinning or thickening. This misclassification may be especially prevalent with partial volume effects at the periosteal surface. Although the increases in bone parameters in the experimental subjects are modest (<1.6%), they are not dissimilar to the magnitude of clinically relevant changes reported by other QCT studies examining interventions for osteoporosis, considering the short time period. For example, postmenopausal women treated with zoledronic acid for 36 months showed a 2.86% increase in integral proximal femur vBMD (Eastell, 2010). This would correspond to a 0.48% change over six months. The in-plane resolution of our CT images, 234 μm/voxel, limits the degree to which changes can be detected after 28 weeks (196 days) as human mineral apposition rate is reported to be around 0.5 to 1 μm/day (Cowin, 2001). The CT scanner, like most devices, is susceptible to repeatability errors over time, and may be responsible for some of the changes observed here. The repeatability of the quantitative analysis of the scans was improved by collecting CT data for control and experimental subjects concurrently, as well as by using the phantom. However, the phantom may not account all of the variability. A fixed amount of hydroxyapatite was scanned with a subset of the scans to determine the repeatability error in the QCT analysis over time. The density calculated from the CT scans varied minimally with a coefficient of variation of 0.85% over 6 months.

The relationship between BMD and fracture risk is exponential, a relatively small change in BMD can be expected to have a very large effect on fracture risk (Faulkner, 2000). This effect has been shown in pharmacological intervention studies. For example, daily oral dose of Ibandronate in post-menopausal women resulted in 2.8% increase in femoral neck BMD and 6.5% increase in lumbar spine BMD, and corresponded to a 49% decrease in relative fracture risk over 3 years (Chesnut, 2004). In another study, a 1.2% increase in spinal BMD resulted in a 36% reduction in vertebral fracture rates over 3 years. Hence, the small decrease in the control group, and a small increase (or prevention of the decrease) in the experimental group in this study may be clinically significant.

In addition to the relatively short time period and CT resolution, the loading protocol given to subjects was relatively modest. A three day per week, 50 cycles per day protocol was initially selected based on animal literature suggesting there was little benefit to loading more often or with more cycles (Rubin and Lanyon, 1984, Robling, 2000). However, more recent literature indicates that in humans, five day per week interventions result in measurably larger osteogenic responses than do three day per week interventions (Bailey, 2010). Similarly, our own more recent calculations based on the experimental data and the Daily Strain Stimulus theory suggest that there may be substantial benefit applying 100 loading cycles per day rather than only 50 cycles per day (Bhatia, 2013).

The hypothesis that the adaptation response is strain-magnitude related was based on animal literature. A strain dependent response and not force dependent response was observed in this study. To our knowledge this relation has previously only been shown using animal models as discussed in the literature review. The strains acting within a bone depends not only on the applied force, but also on the shape of the bone and the density distribution within the bone.

Hence, assigning a fixed force based loading protocol is unreasonable, and the forces assign should account for biological variability in bone shape, size and density distribution between subjects. Here, only a subset of subjects was assigned target loads to achieve a predefined target strain based on individual anatomy. In the future, a target strain based approach should be used to reduce the variability in the observed adaptation response.

In summary, we have developed an *in vivo* loading model of the human radius for the purpose of understanding how mechanical loading characteristics influence bone adaptation. We have shown that an increase (or the prevention of a decrease) in ultra-distal radius size and mass was the primary adaptation response to axial compression of the radius, and may be clinically significant. In addition to its usefulness as a model system for exploring bone adaptation in humans, mechanical loading protocols such as the one described may be an effective means of strengthening the distal radius of women.

Chapter 5. Aim 3

Determine the degree to which local adaptation within a given bone depends on the local mechanical environment, by comparing local adaptation with the corresponding strains.

5.1 Introduction

In theory, bone remains in a balanced state until the localized strain environment changes above (or below) some threshold (Frost, 1983). The strain environment in a bone for an applied load depends on the shape and density distribution of mineral within the bone. Therefore, for an applied force, the strains observed within the bone will be different at different locations. The coupled action of osteoclasts and osteoblasts during remodeling is known to be a strain-regulated phenomenon (Smit, 2000). The relationship between bone adaptation and mechanical loading environment has been well documented in animal models. A site-specific adaptation response has been observed in response to applied mechanical stimulus in mouse tibiae (Fritton, 2005) suggesting the influence of strain in the bone adaptation response. Bone formation has also been shown to be directly dependent on the magnitude of strain gradient within adult turkey radii (Gross, 1997). Additionally, sclerostin, which is an inhibitor of bone formation, has been found to be mechano-regulated, with regions of higher strains associated with smaller concentrations of sclerostin (Robling, 2008). Collectively, this evidence demonstrates that a strain-structure relation exists within the bone.

The relation between strain and bone adaptation has not been tested in humans, mainly due to the difficulty in assessing the mechanical environment of human bone, as well as the difficulty in accurately quantifying the changes taking place within the bone. However, with the

help of the methods developed and validated in the previous chapters, the relation between the local bone adaptation and the local mechanical environment can now be tested in humans.

The purpose of this study was to determine whether the changes observed in the bone mineral parameters due to the loading protocol are localized to certain regions of the bone, and whether these localized changes are related to the magnitude of the mechanical stimulus experienced by the region. Our hypothesis was that the changes observed would be localized to regions experiencing larger strains or stresses, and these changes would be proportional to the strains or stresses experienced by these regions.

5.2 Methods

5.2.1 Subjects

Subjects who were assigned to the experimental loading protocol (n=23) described previously were used for this study. CT scans from the baseline and 14 week time points, and finite element models of the baseline scan were generated as described in Chapters 3 and 4, and were used to test the hypotheses here. The present analysis focused on data collected at the 14 week time point because that is when maximum changes were observed (see Chapter 4).

The bone masks for the two time points, and the strain and stress maps from the finite element models of the baseline scan were imported into Matlab for each subject. The registration procedure for between time point scans, as described in Chapter 4, had a small scope of error ($0.7 \pm 0.7°$) about the longitudinal axis. To improve the accuracy of the registration, a 2.5 mm thick transverse section immediately proximal to the sub-chondral plate was selected from the radius masks at each of the two time points, and re-registered only about the longitudinal axis (Figure 5-1). A custom code was used to analyze local regions within the bone, and to obtain

changes in bone mineral parameters in these regions, as well as the strains and stresses acting on those regions.

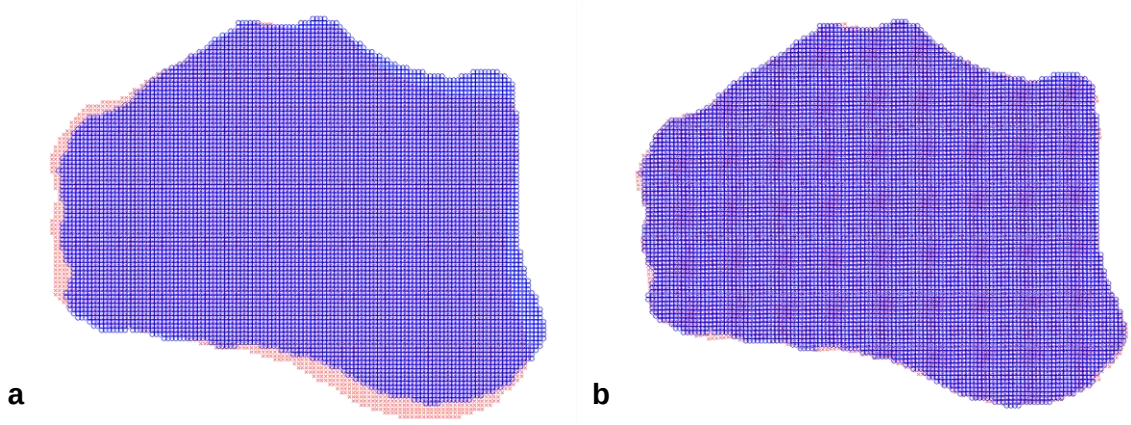

Figure 5-1: a) Unregistered, and b) Registered masks. Blue mask is mask at baseline time point, Red mask is mask at 14 week time point

5.2.2 Region of Interest Selection

A 9.375 mm section just proximal to the sub-chondral plate, as described in Chapter 4, was selected for this analysis, and was divided into four quadrants. Based on the cadaver mechanical testing; high strains were measured on the dorsal surface on the radial and ulnar sides (see Chapter 3). The co-ordinates of the 9.375 mm section were converted from Cartesian to Polar about the centroid of the region, with 0° on the ulnar side, and the angles increasing in the counter-clockwise direction. The four quadrants were defined as all voxels (for CT) and nodes (for FE) corresponding to the region between 0° and 90°, 90° and 180°, 180° and 270°, and 270° and 360° respectively. These corresponded to the, dorsal-ulnar, dorsal-radial, palmar-radial, and palmar-ulnar sides respectively (Figure 5-2), and coincided with these regions of high and low strain observed in the cadaver specimens. Bone mineral parameters i.e. integral bone volume (BV), bone mineral content (BMC), and bone mineral density (BMD) were calculated for these quadrants at both time points. Additionally, principal strains and stresses were averaged for all nodes contained within each of the quadrants. The mechanical parameters, i.e. energy equivalent strains and energy equivalent stress were calculated at baseline as shown below:

Energy equivalent strain: $\bar{\varepsilon} = \sqrt{\frac{2U}{E}}$, Energy equivalent stress: $\bar{\sigma} = \sqrt{2UE}$

where E=elastic modulus, and U=strain energy density, $U = \frac{1}{2}[\sigma_1\varepsilon_1 + \sigma_2\varepsilon_2 + \sigma_3\varepsilon_3]$, ε_n and σ_n are the strain and stress values in the principal direction.

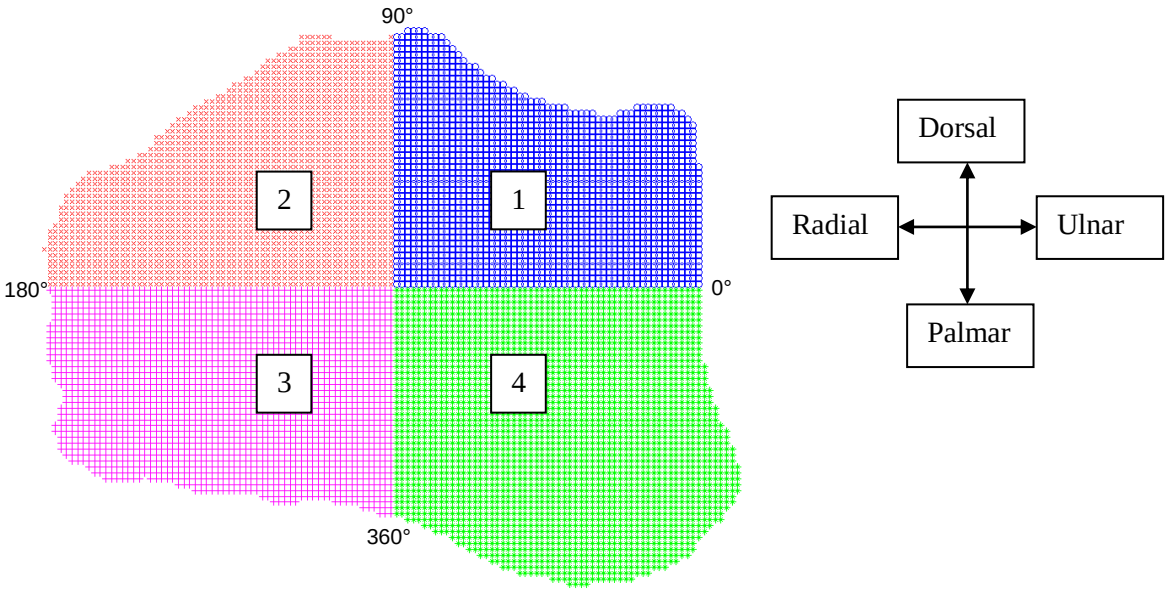

Figure 5-2: Quadrant regions of interest. Number inside each quadrant indicates quadrant number.

5.2.3 Data Analysis

Bone mineral parameters and mechanical parameters were obtained at each quadrant for all subjects. Percent changes in bone parameters were calculated between 14 week and baseline time points at each quadrant, as well as for all quadrants combined. To test the hypothesis that the changes in the bone mineral parameters taking place within the bone are localized, repeated measures ANOVA with quadrant as the main effect was performed on the percent change in bone mineral parameters as well as the values of mechanical parameters. A significant effect of

quadrant on the mechanical parameters would suggest that the mechanical environment acting on the bone is location dependent. A significant effect of quadrant on the percent change in bone mineral parameters would suggest a region-specific adaptation response.

To test the hypothesis that the changes in the bone mineral parameters are related to the mechanical environment experienced by these regions, Pearson's correlations were calculated for percent change is the bone mineral parameters versus the mean energy equivalent strain and the mean energy equivalent stress measures, for each individual subject. Additionally, to account for between-subject variability, the percent changes in bone mineral parameters and the magnitudes of the mechanical parameters were normalized by dividing the individual quadrant values by the average values for the entire region (all quadrants combined) for each subject. Pearson's correlations for the normalized percent changes in bone mineral parameters versus the normalized mechanical parameters were then calculated for all subjects combined.

5.3 Results

The average volume of each quadrant was 0.95 ± 0.1 cm^3, and corresponded to 27760 ± 2922 voxels and 2935 ± 349 nodes. The average values of percent change in the bone mineral parameters, and the average values of the mechanical parameters for each quadrant are shown in Table 5-1. The mechanical parameters and the changes in bone mineral parameters matched the changes observed in Chapter 4. As expected, a significant effect of quadrant was observed for energy equivalent strain and energy equivalent stress ($p<0.001$), however, no effect of quadrant was observed for any of the changes in bone mineral parameters. The mechanical parameters were largest in quadrant 1 and smallest in quadrant 4, and corresponded to the respective largest and smallest changes in BMD (Figure 5-3).

Table 5-1: Mean (S.D) of Energy equivalent strain, Energy equivalent stress, and percent changes in BMD, BMC and BV at the four quadrant regions

Quadrant	Energy Equivalent Strain (με)	Energy Equivalent Stress (MPa)	Percent change in BMD (%)	Percent change in BMC (%)	Percent change in BV (%)
1	1114 (470)	1.652 (0.31)	0.484 (2.43)	1.214 (2.27)	0.752 (2.15)
2	1069 (515)	1.414 (0.34)	0.36 (2.92)	0.9 (3.43)	0.57 (2.26)
3	616 (274)	0.711 (0.21)	0.35 (2.12)	1.234 (3.05)	0.901 (2.52)
4	542 (247)	0.708 (0.27)	0.327 (2.12)	1.202 (3.86)	0.859 (2.73)
Total	835 (376)	1.121 (0.28)	0.380 (2.15)	1.138 (3.16)	0.771 (2.25)

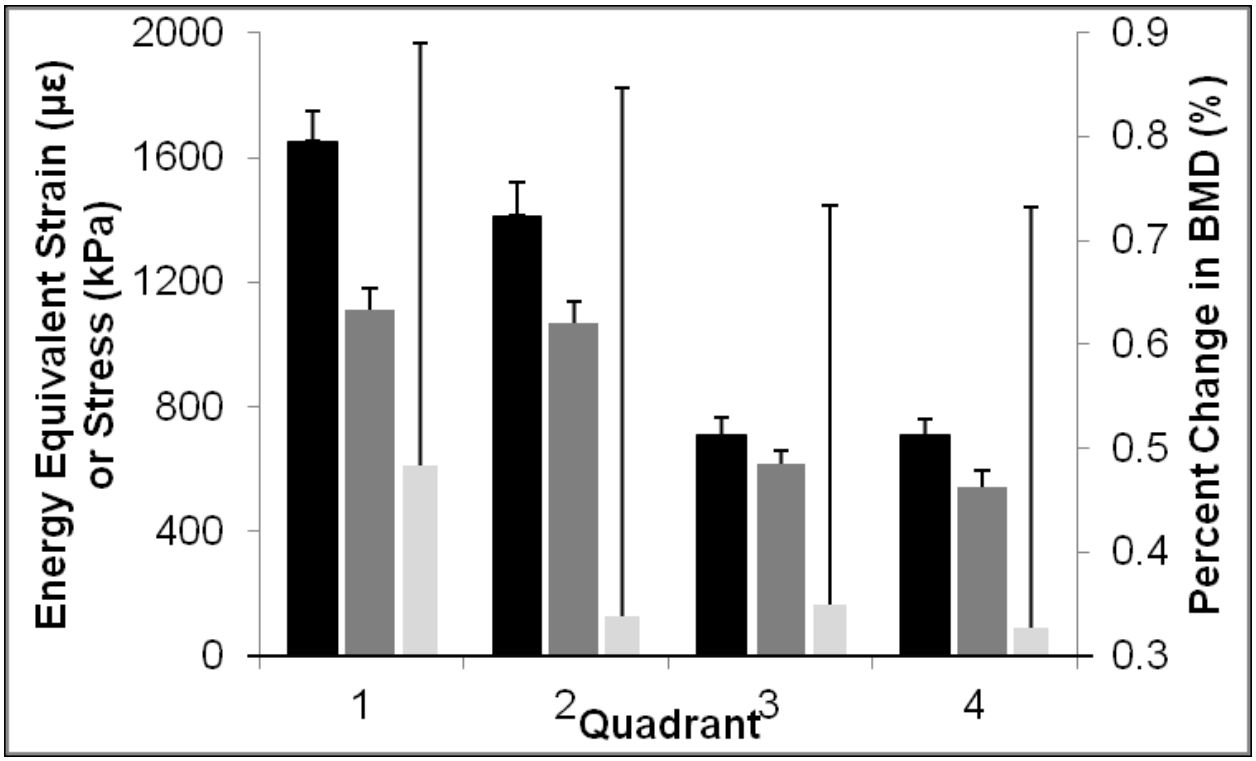

Figure 5-3: Energy equivalent strain (black), Energy equivalent stress (dark grey), and Percent change in BMD (light grey) at the four quadrant regions

Figure 5-4 shows that there was considerable between-subject variability in the raw percent change in BMD versus raw energy equivalent stress. Histograms of the correlation values for percent change in BMD versus energy equivalent strain, and versus energy equivalent stress for each individual subject are shown in Figure 5-5. For all subjects combined, a small but significant correlation was observed between the normalized percent change in BMD and normalized mean energy equivalent strain ($r=0.333$, $p=0.002$), and normalized mean energy

equivalent stress (r=0.353, p=0.001; Figure 5-6). Percent changes in BMC and BV were not correlated to either of the mechanical parameters (-0.15<r<0.1, p>0.1).

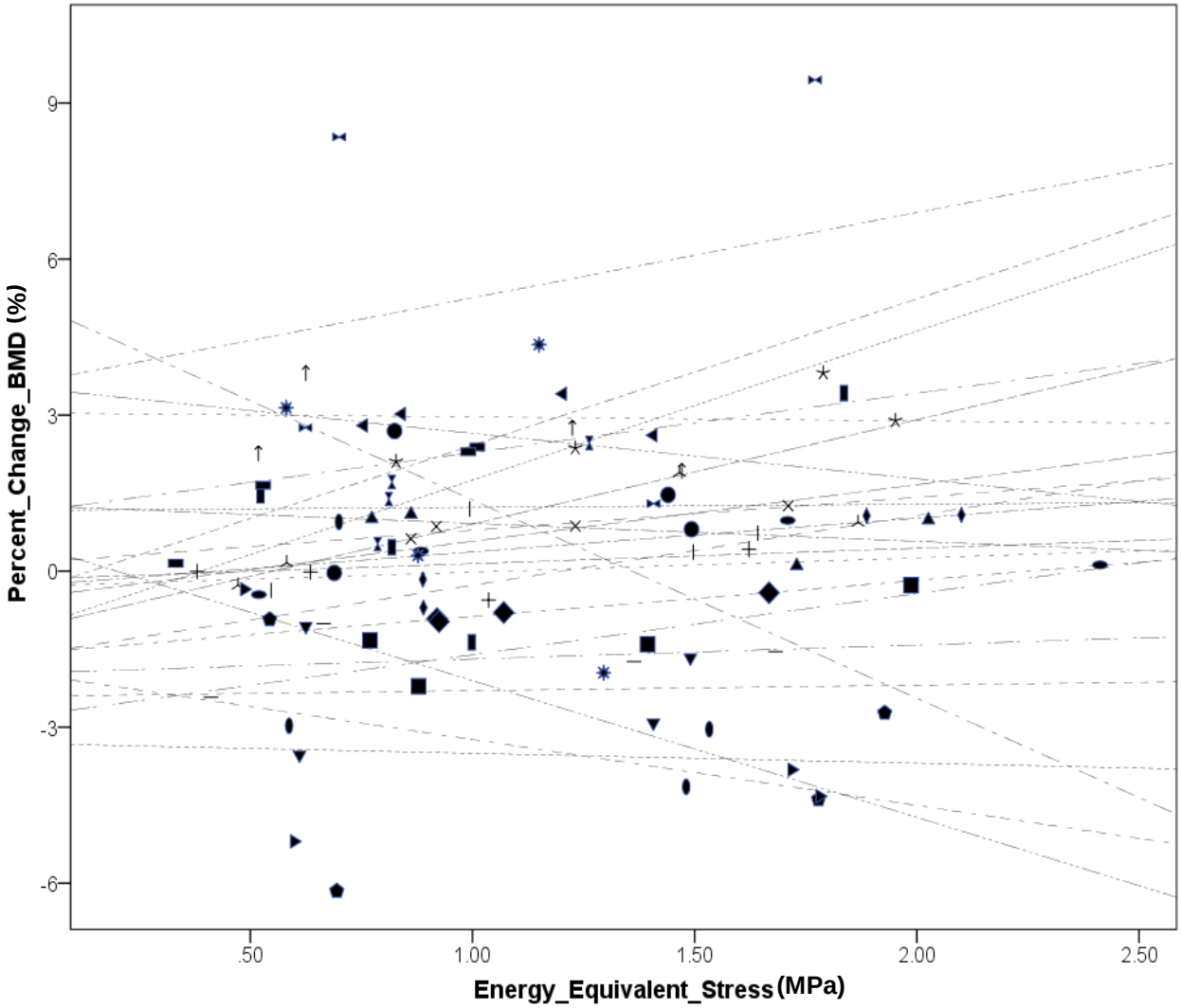

Figure 5-4: Plot of Percent change in BMD (%) versus the Energy Equivalent Stress (MPa). Each symbol corresponds to a subject. The dashed lines are the regression lines for each subject.

a) 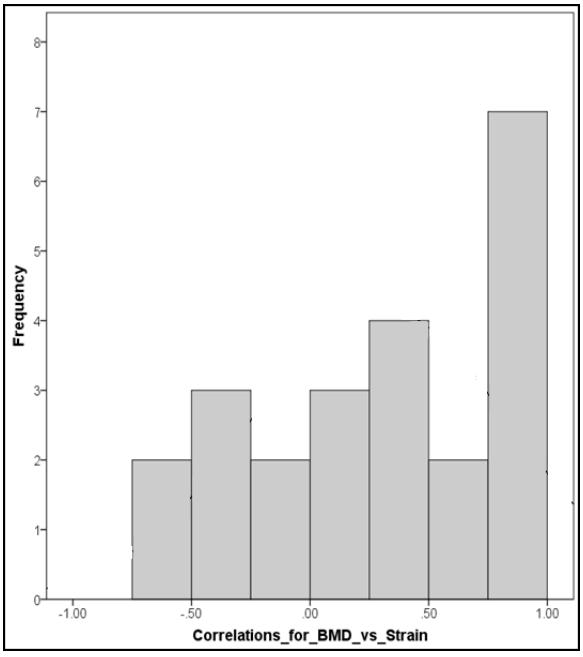

b) 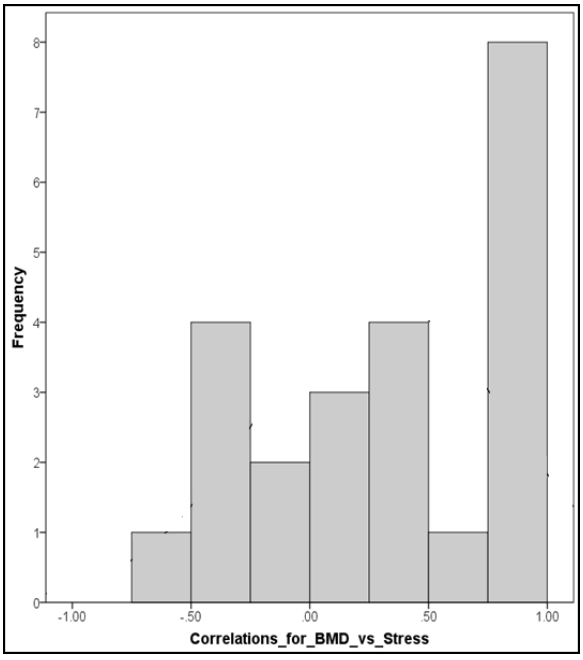

Figure 5-5: Histogram of Pearson's r correlations between a) percent change in BMD and energy equivalent strain, and b) percent change in BMD and energy equivalent stress, for all subjects.

a)

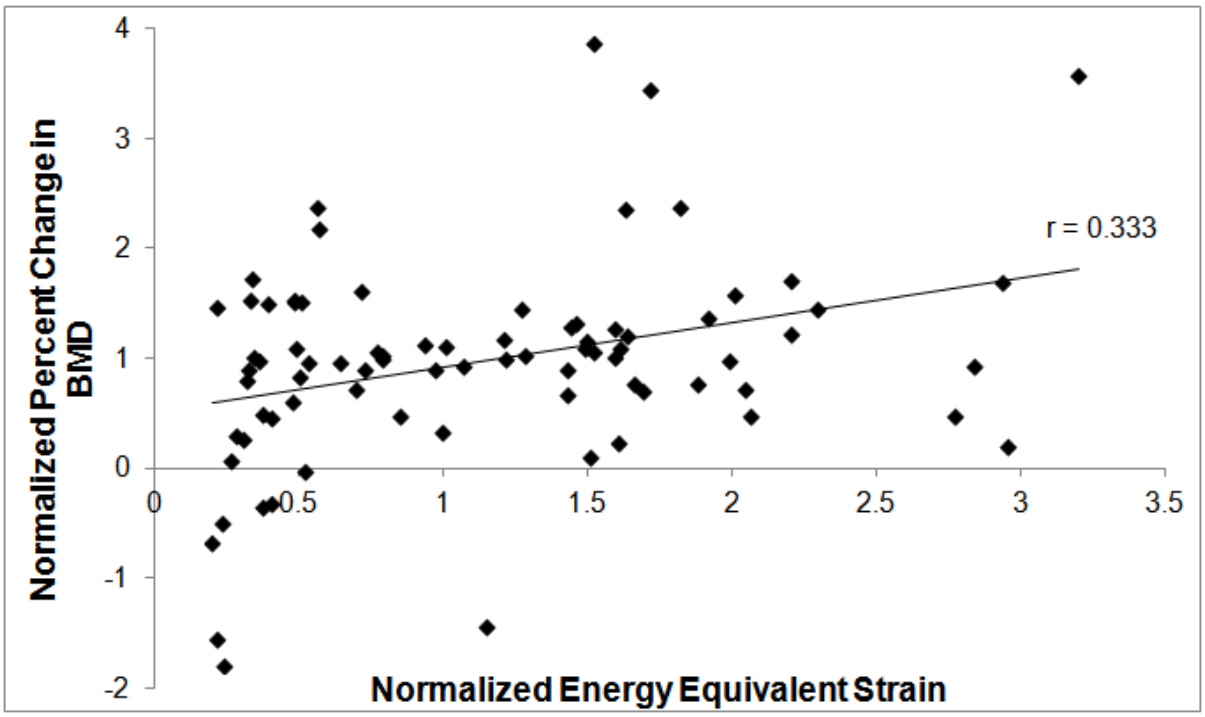

b)

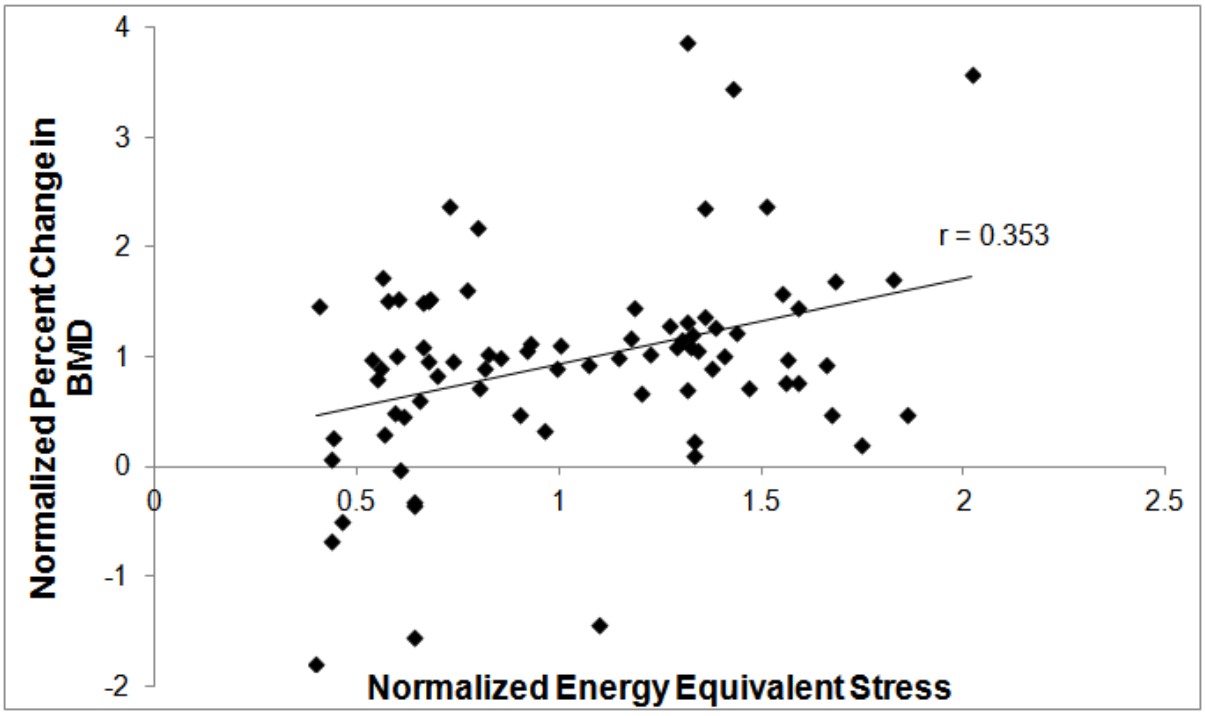

Figure 5-6: Plot of normalized percent change in BMD versus a) normalized energy equivalent strain, and b) normalized energy equivalent stress

5.4 Discussion

The purpose of this study was to test whether the changes observed in bone mineral parameters, due to an applied mechanical stimulus, were localized to certain regions of the bone. We hypothesized that the changes observed on account of the adaptive response would be site specific. Additionally, these localized changes were expected to be dependent upon the magnitude of the mechanical stimulus experienced by the local region.

Our hypothesis that the changes in bone parameters would be site specific was not supported. The quadrants selected for the analysis were based on cadaver testing data and these locations corresponded to the highest surface strains during our loading task, which were measured on the dorsal surface on the radial and ulnar sides. We could have positioned the quadrants in the anatomical positions, i.e. corresponding to the ulnar, dorsal, radial, and palmar regions. However, according to our preliminary analysis, the highest energy equivalent strain and stress values were observed in the current quadrants 1 and 2 corresponding to the dorsal-ulnar and dorsal-radial regions. Based on our hypothesis that the largest changes in the bone mineral parameters will be localized to the regions experiencing the largest mechanical stimulus, the position of these quadrants is likely better suited for the analysis.

The voxel size of the CT scans used in this study was 0.234 mm X 0.234 mm X 0.625 mm, and the average volume of the each quadrant was 0.95 ± 0.1 cm^3 (27760 voxels). At this resolution the volumes of interest may be too small to accurately measure the changes taking place in the quadrants. However, preliminary analysis on the repeatability of measuring localized changes showed that changes in BMD were highly repeatable with a coefficient of variance of less than 1%, and the coefficient of variance for localized changes in BMC and BV was about

2%. Therefore these methods should be capable of measuring the changes taking place in each quadrant with reasonable accuracy.

The standard deviations for changes in bone parameters were relatively high compared to the average percent changes over all subjects (Table 5-1). Percent change in BMD versus energy equivalent stress is plotted for each subject in Figure 5-4, and the relation observed was different for different subjects. This suggests that that the adaptive response was subject-specific; some subjects responded to loading task while some did not. It is also possible that although the response could be site specific, the sites at which the largest (or smallest) changes occurred may differ between subjects, resulting in an inability to detect a single quadrant with the largest or smallest changes. Power analysis was performed based on pilot data to determine the number of subjects needed in each group, and resulted in n=10 subjects per group. However, that analysis was based on being able to detect changes on the whole bone BMC of 1%, and not the local changes measured here. The post-hoc observed power for the site-specific response analysis was less than 0.1. Therefore, the number of subjects used here was insufficient to detect a site specific response.

The distribution for correlation values (Figure 5-5) also suggests a subject specific behavior. The subjects showing a weak correlation ($r<0.5$) had an average percent change of 0.04 ± 2.7 % in whole section BMD compared to 0.78 ± 1.1 % for the subjects with stronger correlations ($r>=0.5$). To account for between-subject variability, the percent change in bone mineral parameters, and the magnitudes of the mechanical parameters at each quadrant were normalized to the mean values for the entire section of the four quadrants combined. After normalization, a significant correlation was observed between percent change in BMD and the energy equivalent strain and stress (Figure 5-6). However, these correlations were very small and

may not be very meaningful. It is possible that a relation between localized changes and localized mechanical environment exists but cannot be confidently determined using the current methods.

The individual correlations for each subject were calculated using only four points (quadrants), and increasing the number of local analysis regions would improve the accuracy of this relation. However, increasing the number of regions would also result in a decrease in the volume of each region, and on account of the relatively large voxel size, reduce the reliability of the changes measured in the regions. Future studies should use high resolution pQCT data, a more strenuous mechanical stimulus, and more local analysis regions to get a more reliable and accurate detection of the relation between the local changes taking place within the bone and the local mechanical environment.

In conclusion, despite the limitations of this study, small but significant correlations were observed between changes in BMD and energy equivalent strain and stress. Although these relations were very small and may not be very meaningful, to our knowledge, this is the first time that the localized adaptation behavior of bone has been tested in humans. Apart from being a useful tool to quantify the relation between localized changes taking place within the bone and the localized mechanical environment, these methods may be useful for predicting the location of changes taking place within the bone during a novel loading task.

Chapter 6. Study Summary, Future Work, and Conclusion

The purpose of this research was to quantify the relationship between structural adaptations in human bone and its mechanical environment, with the long term goal of designing and evaluating exercise interventions to a) prevent or slow bone loss that can lead to osteoporosis and increased fracture risks, b) increase peak bone mass, and/or bone structural properties earlier in life to improve fracture strength.

A novel *in-vivo* wrist loading model, wherein young women leaned onto the palm of their hand to apply axial loads onto their radius, was used to accomplish aims of this research. Methods for subject specific finite element model generation to predict the surface strains experienced by the distal radius during this loading activity were validated by comparing experimentally measured strains with model predicted strains. This **validated modeling method can accurately (r=0.968, RMSE=11.1%) and non-invasively predict periosteal strains acting on the radius during the loading task.** The validated model was used to assess loading-induced bone strain in the subjects recruited for this study. The FE model validation was based on experimental data from 4 cadaveric specimens, and additional samples could improve the accuracy of the predictions and reduce the RMSE.

At the end of the 28 week loading protocol, small but significant decreases in bone parameters were observed in subjects of the control group, however, increases or no changes were observed for subjects of the exercise group. **An increase (or the prevention of a decrease) in ultra-distal radius size and mass was the primary adaptation response to axial compression** of the radius, and the increases were attributed to **periosteal bone formation in the ultra-distal region.** In addition, this **adaptation response was more directly related to the**

strain magnitude than the force magnitude of the applied stimulus, suggesting that exercise regimes should be subject-specific, and should account for biological variability in bone shape, size and density distribution of the subject.

Here, subjects were assigned a relatively modest loading protocol that resulted in a non-uniform adaptation response. Future work may be more successful if the loading protocol were more vigorous, e.g. 100 loading cycles a day for 5 days a week rather than 50 loading cycles 3 days a week. Bone formation rate in humans is reported to be around 0.5-1μm/day. The present study quantified changes over 28 weeks, and may not be a sufficient time to detect some of the expected changes. A longer duration of the loading protocol should be investigated in the future. Subject compliance was significantly reduced during the second half of the loading protocol resulting in a reduced response from 14 to 28 weeks. To improve the efficacy of such exercise protocols, methods to improve long term subject compliance must be investigated. Additionally, subject compliance was quantified using self reported logs. A subset of subjects used a custom built loading device that digitally recorded the loading data and acted as a check for compliance. This loading device should be used by all subjects in future studies.

For an applied force, the strains observed within the bone are different within different regions on account of the shape of the bone and the mineral density distribution within the bone. Due to these differences, site-specific bone adaptation was expected in the subjects, with the greatest amount of bone being added at locations experiencing the highest strains. **Between subject variability and a relatively low CT resolution prevented the detection of this site-specific behavior.** However, after controlling for between subject variability, **a small but significant correlation was observed between changes in BMD and the magnitude of the energy equivalent strain and stress measures within the bone.** Although a strain-dependant

site-specific behavior has previously been shown in animals, to our knowledge, **this was the first time that the localized adaptation behavior of bone was tested in humans.**

The resolution of the CT scans used for our analyses here was relatively low for some of the analysis. High resolution CT (HR-pQCT) data could improve the accuracy and repeatability of measuring localized changes in the bone parameters, and should be used for future studies. The HR-pQCT data could also be used to create FE models capable of predicting strain at the trabecular level, which could be used to further analyze the local strain-adaptation response.

Apart from magnitude of the applied stimulus, bone adaptive response is also affected by loading rate and frequency; an increased response is observed with increase in rate and/or frequency. With *in vivo* loading, the magnitude of the applied stimulus can only be increased to a certain extent. Varying the loading rate and frequency could increase the effective stimulus required for the bone to adapt. The magnitude, frequency, and rate of the applied stimulus can be obtained for each subject using the portable loading device. This loading data can be used in conjunction with the Strain or Stress Stimulus theories to predict changes taking place within the bone at the local level.

In conclusion, we have developed an *in vivo* loading model of the human radius for the purpose of understanding influence of mechanical environment on bone adaptation. The loading task was capable of producing an osteogenic response, and along with the validated *in-vivo* FE model, we were able to test the relation between the mechanical characteristics of the applied loads and the resultant changes in the bone mineral parameters. In addition to its usefulness for exploring bone adaptation in humans, this research also acts as a step towards designing effective targeted mechanical interventions to increase (or prevent the decrease of) bone strength.

Cited Literature

1. Adams, D. J., Spirt, A. A., Brown, T. D., Fritton, S. P., Rubin, C. T., & Brand, R. A. (1997). Testing the daily stress stimulus theory of bone adaptation with natural and experimentally controlled strain histories. Journal of biomechanics, 30(7), 671-678.

2. Adami, S., Gatti, D., Braga, V., Bianchini, D., & Rossini, M. (1999). Site-Specific Effects of Strength Training on Bone Structure and Geometry of Ultradistal Radius in Postmenopausal Women. Journal of Bone and Mineral Research, 14(1), 120-124

3. Ahola, R., Korpelainen, R., Vainionpää, A., Leppäluoto, J., & Jämsä, T. (2009). Time-course of exercise and its association with 12-month bone changes. BMC musculoskeletal disorders, 10(1), 138.

4. Anderson, D. D., Deshpande, B. R., Daniel, T. E., & Baratz, M. E. (2005). A three-dimensional finite element model of the radiocarpal joint: distal radius fracture step-off and stress transfer. The Iowa orthopaedic journal, 25, 108.

5. Anderson, A. E., Ellis, B. J., Maas, S. A., Peters, C. L., & Weiss, J. A. (2008). Validation of finite element predictions of cartilage contact pressure in the human hip joint. Journal of biomechanical engineering, 130(5), 051008.

6. Armstrong, C. G., Lai, W. M., & Mow, V. C. (1984). An analysis of the unconfined compression of articular cartilage. Journal of biomechanical engineering, 106(2), 165.

7. Bailey, C. A., & Brooke-Wavell, K. (2010). Optimum frequency of exercise for bone health: randomised controlled trial of a high-impact unilateral intervention. Bone, 46(4), 1043-1049.

8. Beaupré, G. S., Orr, T. E., & Carter, D. R. (1990). An approach for time-dependent bone modeling and remodeling—theoretical development. Journal of Orthopaedic Research, 8(5), 651-661.

9. Bergstralh, E. J., Offord, K. P., Sinaki, M., Wahner, H. W., & Melton, L. J. (1990). Effect of season on physical activity score, back extensor muscle strength, and lumbar bone mineral density. Journal of Bone and Mineral Research, 5(4), 371-377.

10. Bhatia, V. A., Edwards, W. B., Troy, K. L. (2012). Repeatability of image registration and segmentation procedures for ct scans of the human distal radius. Proceedings of the American Society of Biomechanics, Gainesville, FL.

11. Bhatia, V. A., Edwards, W. B., Troy, K. L. (2013). Predicting bone adaptation at the human distal radius using cadaveric specimens and the daily strain stimulus theory. Proceedings of the 59th Annual Meeting of the Orthopaedic Research Society, San Antonio, TX.

12. Bonewald, L. F. (2006). Mechanosensation and transduction in osteocytes. BoneKEy-Osteovision, 3(10), 7-15.

13. Brekelmans, W. A. M., Poort, H. W., & Slooff, T. J. J. H. (1972). A new method to analyse the mechanical behaviour of skeletal parts. Acta Orthopaedica, 43(5), 301-317.

14. Carter, D. R., & Hayes, W. C. (1977). The compressive behavior of bone as a two-phase porous structure. The Journal of bone and joint surgery. American volume, 59(7), 954-962.

15. Carter, D. R. (1987). Mechanical loading history and skeletal biology. Journal of biomechanics, 20(11), 1095-1109.

16. Chen, J. C., Beaupré, G. S., & Carter, D. R. (2010). An approach to quantifying bone overloading and hypertrophy with applications to multiple experimental studies. Bone, 46(2), 322-329.

17. Chesnut, C. H., Skag, A., Christiansen, C., Recker, R., Stakkestad, J. A., Hoiseth, A., & Delmas, P. D. (2004). Effects of oral ibandronate administered daily or intermittently on fracture risk in postmenopausal osteoporosis. Journal of bone and mineral research, 19(8), 1241-1249.

18. Cowin, S. C. (Ed.). (2001). Bone mechanics handbook, 2nd ed. Boca Raton: CRC press.

19. Dalstra, M., Huiskes, R., Odgaard, A., & Van Erning, L. (1993). Mechanical and textural properties of pelvic trabecular bone. Journal of biomechanics, 26(4), 523-535.

20. De Souza, R. L., Matsuura, M., Eckstein, F., Rawlinson, S. C., Lanyon, L. E., & Pitsillides, A. A. (2005). Non-invasive axial loading of mouse tibiae increases cortical bone formation and modifies trabecular organization: a new model to study cortical and cancellous compartments in a single loaded element. Bone, 37(6), 810-818.

21. Dolan, S. H., Williams, D. P., Ainsworth, B. E., & Shaw, J. M. (2006). Development and reproducibility of the bone loading history questionnaire. Medicine and science in sports and exercise, 38(6), 1121.

22. Ducher, G., Courteix, D., Meme, S., Magni, C., Viala, J. F., & Benhamou, C. L. (2005). Bone geometry in response to long-term tennis playing and its relationship with muscle volume: a quantitative magnetic resonance imaging study in tennis players. Bone, 37(4), 457-466.

23. Eastell, R., Lang, T., Boonen, S., Cummings, S., Delmas, P. D., Cauley, J. A., & Black, D. M. (2010). Effect of once-yearly zoledronic acid on the spine and hip as measured by quantitative computed tomography: results of the HORIZON Pivotal Fracture Trial. Osteoporosis international, 21(7), 1277-1285.

24. Edwards, W. B., & Troy, K. L. (2012). Finite element prediction of surface strain and fracture strength at the distal radius. Medical engineering & physics, 34(3), 290-298.

25. Faulkner, K. G. (2000). Bone matters: are density increases necessary to reduce fracture risk? Journal of Bone and Mineral Research, 15(2), 183-187.

26. Földhazy, Z., Arndt, A., Milgrom, C., Finestone, A., & Ekenman, I. (2005). Exercise-induced strain and strain rate in the distal radius. Journal of Bone & Joint Surgery, British Volume, 87(2), 261-266.

27. Fritton, J. C., Myers, E. R., Wright, T. M., & Van der Meulen, M. C. H. (2005). Loading induces site-specific increases in mineral content assessed by microcomputed tomography of the mouse tibia. Bone, 36(6), 1030-1038.

28. Frost, H. M. (1964). The laws of bone structure. Springfield: Thomas.

29. Frost, H. M. (1983). A determinant of bone architecture: the minimum effective strain. Clinical orthopaedics and related research, 175, 286-292.

30. Genc, K. O., Humphreys, B. T., & Cavanagh, P. R. (2009). Enhanced daily load stimulus to bone in spaceflight and on earth. Aviation, space, and environmental medicine, 80(11), 919-926.

31. Glucksmann, A. (1942). The role of mechanical stresses in bone formation in vitro. Journal of anatomy, 76(Pt 3), 231.

32. Gómez-Cabello, A., Ara, I., González-Agüero, A., & Casajús, J. A. (2012). Effects of Training on Bone Mass in Older Adults. Sports Medicine, 42(4), 301-325.

33. Gross, T. S., Edwards, J. L., Mcleod, K. J., & Rubin, C. T. (1997). Strain gradients correlate with sites of periosteal bone formation. Journal of Bone and Mineral Research, 12(6), 982-988.

34. Gross, T. S., Srinivasan, S., Liu, C. C., Clemens, T. L., & Bain, S. D. (2002). Noninvasive loading of the murine tibia: an in vivo model for the study of mechanotransduction. Journal of Bone and Mineral Research, 17(3), 493-501.

35. Gupta, S., van der Helm, F. C., Sterk, J. C., Van Keulen, F., & Kaptein, B. L. (2004). Development and experimental validation of a three-dimensional finite element model of the human scapula. Proceedings of the Institution of Mechanical Engineers, Part H: Journal of Engineering in Medicine, 218(2), 127-142.

36. Hansen, S., Beck Jensen, J. E., Rasmussen, L., Hauge, E. M., & Brixen, K. (2010). Effects on bone geometry, density, and microarchitecture in the distal radius but not the tibia in women with primary hyperparathyroidism: A case-control study using HR-pQCT. Journal of Bone and Mineral Research, 25(9), 1941-1947.

37. Henry, Y. M., Fatayerji, D., & Eastell, R. (2004). Attainment of peak bone mass at the lumbar spine, femoral neck and radius in men and women: relative contributions of bone size and volumetric bone mineral density. Osteoporosis international, 15(4), 263-273.

38. ICP-FINITE, Matlab central file exchange (http://www.mathworks.com/matlabcentral/fileexchange/24301-finite-iterative-closest-point) Last accessed 03/01/2012.

39. Keller, T. S. (1994). Predicting the compressive mechanical behavior of bone. Journal of biomechanics, 27(9), 1159-1168.

40. Kertis, J. D. (2012). Biomechanical Evaluation of an Optical System for Quantitative Human Motion Analysis.

41. Keyak, J. H., Meagher, J. M., Skinner, H. B., & Mote Jr, C. D. (1990). Automated three-dimensional finite element modelling of bone: a new method. Journal of biomedical engineering, 12(5), 389-397.

42. Keyak, J. H., Fourkas, M. G., Meagher, J. M., & Skinner, H. B. (1993). Validation of an automated method of three-dimensional finite element modelling of bone. Journal of Biomedical Engineering, 15(6), 505-509.

43. Kirmani, S., Christen, D., van Lenthe, G. H., Fischer, P. R., Bouxsein, M. L., McCready, L. K., & Khosla, S. (2009). Bone structure at the distal radius during adolescent growth. Journal of Bone and Mineral Research, 24(6), 1033-1042.

44. Kobayashi, M., Berger, R. A., Nagy, L., Linscheid, R. L., Uchiyama, S., Ritt, M., & An, K. N. (1997). Normal kinematics of carpal bones: a three-dimensional analysis of carpal bone motion relative to the radius. Journal of biomechanics, 30(8), 787-793.

45. Koch, J. C. (1917). The laws of bone architecture. American Journal of Anatomy, 21(2), 177-298.

46. Kriska, A. M., Sandler, R. B., Cauley, J. A., Laporte, R. E., Hom, D. L., & Pambianco, G. (1988). The assessment of historical physical activity and its relation to adult bone parameters. American journal of epidemiology, 127(5), 1053-1063.

47. Lang, T., LeBlanc, A., Evans, H., Lu, Y., Genant, H., & Yu, A. (2004). Cortical and Trabecular Bone Mineral Loss From the Spine and Hip in Long-Duration Spaceflight. Journal of Bone and Mineral Research, 19(6), 1006-1012.

48. Lanyon, L. E., Hampson, W. G. J., Goodship, A. E., & Shah, J. S. (1975). Bone deformation recorded in vivo from strain gauges attached to the human tibial shaft. Acta Orthopaedica, 46(2), 256-268.

49. Lanyon, L. E., & Rubin, C. T. (1984). Static vs dynamic loads as an influence on bone remodelling. Journal of biomechanics, 17(12), 897-905.

50. Lynch, D. J., Birk, T. J., Weaver, M. T., Gohara, A. F., Leighton, R. F., Repka, F. J., & Walsh, M. E. (1992). Adherence to exercise interventions in the treatment of hypercholesterolemia. Journal of behavioral medicine, 15(4), 365-377.

51. Majima, M., Horii, E., Matsuki, H., Hirata, H., & Genda, E. (2008). Load transmission through the wrist in the extended position. The Journal of hand surgery, 33(2), 182-188.

52. Marshall, L. M., Lang, T. F., Lambert, L. C., Zmuda, J. M., Ensrud, K. E., & Orwoll, E. S. (2006). Dimensions and volumetric BMD of the proximal femur and their relation to age among older US men. Journal of Bone and Mineral Research, 21(8), 1197-1206.

53. Meier, C., Woitge, H. W., Witte, K., Lemmer, B., & Seibel, M. J. (2004). Supplementation With Oral Vitamin D3 and Calcium During Winter Prevents Seasonal Bone Loss: A

Randomized Controlled Open-Label Prospective Trial. Journal of Bone and Mineral Research, 19(8), 1221-1230.

54. Moojen, T. M., Snel, J. G., Ritt, M. J. P. F., Kauer, J. M. G., Venema, H. W., & Bos, K. E. (2002). Three-dimensional carpal kinematics in vivo. Clinical Biomechanics, 17(7), 506-514.

55. Morgan, E. F., Bayraktar, H. H., & Keaveny, T. M. (2003). Trabecular bone modulus–density relationships depend on anatomic site. Journal of biomechanics, 36(7), 897-904.

56. Mikić, B., & Carter, D. R. (1995). Bone strain gage data and theoretical models of functional adaptation. Journal of biomechanics, 28(4), 465-469.

57. Nikander, R., Sievänen, H., Heinonen, A., & Kannus, P. (2005). Femoral neck structure in adult female athletes subjected to different loading modalities. Journal of Bone and Mineral Research, 20(3), 520-528.

58. O'Connor, J. A., Lanyon, L. E., & MacFie, H. (1982). The influence of strain rate on adaptive bone remodelling. Journal of Biomechanics, 15(10), 767-781.

59. Pasco, J. A., Henry, M. J., Kotowicz, M. A., Sanders, K. M., Seeman, E., Pasco, J. R., & Nicholson, G. C. (2004). Seasonal periodicity of serum vitamin D and parathyroid hormone, bone resorption, and fractures: the Geelong Osteoporosis Study. Journal of bone and mineral research, 19(5), 752-758.

60. Pauwels, F. (1980). Biomechanics of the locomotor apparatus: contributions on the functional anatomy of the locomotor apparatus. New York: Springer-Verlag.

61. Rantalainen, T., Hoffrén, M., Linnamo, V., Heinonen, A., Komi, P. V., Avela, J., & Nindl, B. C. (2011). Three-month bilateral hopping intervention is ineffective in initiating bone biomarker response in healthy elderly men. European journal of applied physiology, 111(9), 2155-2162.

62. Rapuri, P. B., Kinyamu, H. K., Gallagher, J. C., & Haynatzka, V. (2002). Seasonal changes in calciotropic hormones, bone markers, and bone mineral density in elderly women. Journal of Clinical Endocrinology & Metabolism, 87(5), 2024-2032.

63. Reilly, D. T., & Burstein, A. H. (1975). The elastic and ultimate properties of compact bone tissue. Journal of biomechanics, 8(6), 393-405.

64. Robling, A. G., Burr, D. B., & Turner, C. H. (2000). Partitioning a daily mechanical stimulus into discrete loading bouts improves the osteogenic response to loading. Journal of Bone and Mineral Research, 15(8), 1596-1602.

65. Robling, A. G., Niziolek, P. J., Baldridge, L. A., Condon, K. W., Allen, M. R., Alam, I., & Turner, C. H. (2008). Mechanical stimulation of bone in vivo reduces osteocyte expression of Sost/sclerostin. Journal of Biological Chemistry, 283(9), 5866-5875.

66. Rubin, C. T., & Lanyon, L. E. (1984). Regulation of bone formation by applied dynamic loads. J Bone Joint Surg Am, 66(3), 397-402.

67. Rubin, C. T., & Lanyon, L. E. (1985). Regulation of bone mass by mechanical strain magnitude. Calcified tissue international, 37(4), 411-417.

68. Rubin, C. T., & Lanyon, L. E. (1987). Osteoregulatory nature of mechanical stimuli: function as a determinant for adaptive remodeling in bone. Journal of Orthopaedic Research, 5(2), 300-310.

69. Schileo, E., Taddei, F., Malandrino, A., Cristofolini, L., & Viceconti, M. (2007). Subject-specific finite element models can accurately predict strain levels in long bones. Journal of biomechanics, 40(13), 2982-2989.

70. Schileo, E., Dall'Ara, E., Taddei, F., Malandrino, A., Schotkamp, T., Baleani, M., & Viceconti, M. (2008). An accurate estimation of bone density improves the accuracy of subject-specific finite element models. Journal of biomechanics, 41(11), 2483-2491.

71. Schuind, F., Cooney, W. P., Linscheid, R. L., An, K. N., & Chao, E. Y. S. (1995). Force and pressure transmission through the normal wrist. A theoretical two-dimensional study in the posteroanterior plane. Journal of biomechanics, 28(5), 587-601.

72. Silva, M. J., & Brodt, M. D. (2008). Mechanical stimulation of bone formation is normal in the SAMP6 mouse. Calcified tissue international, 82(6), 489-497.

73. Smit, T. H., & Burger, E. H. (2000). Is BMU-coupling a strain-regulated phenomenon? A finite element analysis. Journal of Bone and Mineral Research, 15(2), 301-307.

74. Srinivasan, S., Weimer, D. A., Agans, S. C., Bain, S. D., & Gross, T. S. (2002). Low-Magnitude Mechanical Loading Becomes Osteogenic When Rest Is Inserted Between Each Load Cycle. Journal of Bone and Mineral Research, 17(9), 1613-1620.

75. Srinivasan, S., Gross, T. S., & Bain, S. D. (2012). Bone mechanotransduction may require augmentation in order to strengthen the senescent skeleton. Ageing research reviews, 11(3), 353-360.

76. Sztefek, P., Vanleene, M., Olsson, R., Collinson, R., Pitsillides, A. A., & Shefelbine, S. (2010). Using digital image correlation to determine bone surface strains during loading and after adaptation of the mouse tibia. Journal of biomechanics, 43(4), 599-605.

77. Taaffe, D. R., Robinson, T. L., Snow, C. M., & Marcus, R. (1997). High-Impact Exercise Promotes Bone Gain in Well-Trained Female Athletes. Journal of bone and mineral research, 12(2), 255-260.

78. Taddei, F., Cristofolini, L., Martelli, S., Gill, H. S., & Viceconti, M. (2006). Subject-specific finite element models of long bones: an in vitro evaluation of the overall accuracy. Journal of biomechanics, 39(13), 2457-2467.

79. Taddei, F., Schileo, E., Helgason, B., Cristofolini, L., & Viceconti, M. (2007). The material mapping strategy influences the accuracy of CT-based finite element models of bones: an evaluation against experimental measurements. Medical engineering & physics, 29(9), 973-979.

80. Taddei, F., Zavatsky, A. B., Cristofolini, L., & Gill, H. S. (2008). Experimental validation of a finite element model of a human cadaveric tibia. Journal of biomechanical engineering, 130, 031016-1.

81. Torrance, A. G., Mosley, J. R., Suswillo, R. F. L., & Lanyon, L. E. (1994). Noninvasive loading of the rat ulna in vivo induces a strain-related modeling response uncomplicated by trauma or periostal pressure. Calcified tissue international, 54(3), 241-247.

82. Troy, K. L., Edwards, W. B., Bhatia, V. A., & Bareither, M. L. (2013). In vivo loading model to examine bone adaptation in humans: A pilot study. Journal of Orthopaedic Research.

83. Turner, C. H., Akhter, M. P., Raab, D. M., Kimmel, D. B., & Recker, R. R. (1991). A noninvasive, in vivo model for studying strain adaptive bone modeling. Bone, 12(2), 73-79.

84. Turner, C. H., Forwood, M. R., Rho, J. Y., & Yoshikawa, T. (1994). Mechanical loading thresholds for lamellar and woven bone formation. Journal of bone and mineral research, 9(1), 87-97.

85. Turner, C. H. (1998). Three rules for bone adaptation to mechanical stimuli. Bone, 23(5), 399-407.

86. Umemura, Y., Nagasawa, S., Honda, A., & Singh, R. (2008). High-impact exercise frequency per week or day for osteogenic response in rats. Journal of bone and mineral metabolism, 26(5), 456-460.

87. Viljakainen, H. T., Palssa, A., Karkkainen, M., Jakobsen, J., Cashman, K. D., Molgaard, C., & Lamberg-Allardt, C. (2006). A seasonal variation of calcitropic hormones, bone turnover and bone mineral density in early and mid-puberty girls-a cross-sectional study. British Journal of Nutrition, 96(1), 124-130.

88. Vogt, M. T., Cauley, J. A., Tomaino, M. M., Stone, K., Williams, J. R., & Herndon, J. H. (2002). Distal Radius Fractures in Older Women: A 10-Year Follow-Up Study of Descriptive Characteristics and Risk Factors. The Study of Osteoporotic Fractures. Journal of the American Geriatrics Society, 50(1), 97-103.

89. Warden, S. J., Hurst, J. A., Sanders, M. S., Turner, C. H., Burr, D. B., & Li, J. (2005). Bone adaptation to a mechanical loading program significantly increases skeletal fatigue resistance. Journal of bone and mineral research, 20(5), 809-816.

90. Weeks, B. K., & Beck, B. R. (2008). The BPAQ: a bone-specific physical activity assessment instrument. Osteoporosis International, 19(11), 1567-1577.

91. Wolfe, S. W., Neu, C., & Crisco, J. J. (2000). In vivo scaphoid, lunate, and capitate kinematics in flexion and in extension. The Journal of hand surgery, 25(5), 860-869.

92. Wolff, J. (1892). Das Gesetz der Transformation der Knochen. Hirchwild, Berlin. (Translated as The Law of Bone Remodeling.) Springer, Berlin.

93. Xie, L., Jacobson, J. M., Choi, E. S., Busa, B., Donahue, L. R., Miller, L. M., & Judex, S. (2006). Low-level mechanical vibrations can influence bone resorption and bone formation in the growing skeleton. Bone, 39(5), 1059-1066.

Vita

NAME : Varun Bhatia

EDUCATION

University of Illinois at Chicago, Chicago, IL 2009-2013
Doctor of Philosophy in Bioengineering, **Anticipated July 2013 (GPA: 3.84)**

- Dissertation Title: 'Loading Induced Bone Adaptation in the Distal Radius of Women: Influence of Mechanical Environment'
- Received full tuition research assistantship (2009-present)
- Awarded annual Graduate Student Council Travel Award and Student Presenter Award (2009-2012)
- Member of American Society of Biomechanics (2009-present)

University of Illinois at Chicago, Chicago, IL 2007-2009
Masters in Bioengineering, July 2009 (GPA: 3.88)

- Thesis Title: 'Short Term Bone Adaptation Due to Mechanical Loading in Mouse Tibiae'
- Received full tuition research assistantship (Fall 2008 – Summer 2009)
- Awarded the Graduate College Board of Trustees tuition and fee waiver (Spring 2008)

University of Mumbai, Mumbai, India 2002-2006
Bachelor of Engineering in Biomedical Engineering, May 2006 (GPA: 78%, 95 percentile)

- Senior Design Project: 'Fingerprint Recognition Technique Attendance System'
- Member of IEEE Engineering in Medicine and Biology Society (2003-2006)

INTERNSHIPS

Asian Heart Institute and Research Center, Mumbai, India, 2005
Biomedical Engineering Intern

- Performed preventive maintenance, repair and calibration of medical devices, maintained equipment inventory, and prepared service reports to maximize equipment up-time
- Aided in the optimal set up of medical equipment for a new Neonatal Intensive Care Unit

TEACHING AND RESEARCH EXPERIENCE

University of Illinois at Chicago, Chicago, IL

- **Teaching Assistant** – Biomechanics of the Neuromusculoskeletal System 2011-2012
  Developed grading keys, led discussion sessions, and held reviews for undergraduate and graduate students

- **Research Assistant** - Musculoskeletal Biomechanics Laboratory, 2009-2013
  - Developed methods to analyze and quantify the relationship between bone adaptation and local mechanical environment in human distal radius
  - Designed and fabricated the circuitry and structure for a wrist loading device to record compliance and log forces applied during a loading task
  - Performed mechanical testing of human cadaver bones using a uni-axial material testing machine to measure strains acting on the bones during a specific loading task
  - Processed and analyzed clinical CT imaging data to quantify changes taking place in the human radius bone
  - Developed and validated a subject-specific computational finite element model to predict bone surface strains in the human radius bone using mesh generating tools like 3-Matic, IA-FEMesh, Matlab, and finite-element solvers like Abaqus and FEBio
  - Used mathematical and theoretical models to explain bone adaptation in response to mechanical loading
- **Research Assistant** - Musculoskeletal Biomechanics Laboratory, 2007-2009
  - Designed, developed and validated a low cost, portable, small-scale mechanical testing and loading device capable of testing small samples with high accuracy and precision
  - Implemented a PID control system in LabView to use the testing device in force control and displacement control
  - Used the validated mechanical testing device to measure the stiffness and strength of mouse tibia bones
  - Performed image processing and quantitative analysis of DXA and micro-CT imaging data mouse bones, using image processing and programming packages like Mimics and Matlab
  - Designed fixtures that allowed paired bones to be embedded and precisely aligned for histological analyses
  - Performed histomorphometry analyses on decalcified and un-decalcified bone tissues

RESEARCH AND LABORATORY SKILLS

- Software
  - Finite Element Analysis tools: Abaqus, ANSYS, FEBio, ADINA, 3-Matic, IA-FEMesh, Matlab
  - Image processing: Matlab, Mimics, ImageJ, OsiriX
  - Motion Analysis: Vicon, Motion Analysis Corporation
  - Engineering/Productivity: Matlab, Labview, SPSS, MS office suite
- Laboratory
  - Bone and soft tissue biomechanical testing
  - Digital motion analysis
  - Histological processing

- Animal handling and tissue processing
- Electronic circuit design and fabrication

PEER REVIEWED PUBLICATIONS

1. **Bhatia V.A.**, Troy K.L.: A portable small-scale mechanical loading and testing device: validation and application to a mouse tibia loading model. *Experimental Techniques* (2012)

2. Troy K.L., Edwards W.B., **Bhatia V.A.,** Bareither M.L.: In vivo loading model to examine bone adaptation in humans: A pilot study. *Journal of Orthopaedic Research(2013)*

RECENT CONFERENCE ABSTRACTS

1. **Bhatia V.A.**, Troy K.L.: Mechanical Loading Causes an Acute and Temporary Decrease in the Stiffness and BMC of Mouse Tibiae. Proceedings of the 56th Annual Meeting of the Orthopaedic Research Society, 2010

2. Troy KL, **Bhatia V.A.**: Mechanical loading stimulates localized bone adaptation in the mouse tibia? International Bone and Mineral Society Sun Valley Workshop on Musculoskeletal Biology, August 1-4, 2010

3. **Bhatia V.A.**, Troy K.L.: Mechanical Loading of the Mouse Tibia Stimulates Localized Bone Adaptation. Proceedings of the 34th Annual Conference of the American Society of Biomechanics, 2010

4. **Bhatia V.A.**, Troy K.L.: Alendronate Diminishes the Short Term, Localized Effects of Mechanical Loading in the Tibiae of Female C57bl/6 Mice. Proceedings of the 57th Annual Meeting of the Orthopaedic Research Society, 2011

5. **Bhatia V.A.**, Edwards W.B., Troy K.L.: Effect of image resolution on the accuracy of trabecular morphology and the convergence behavior of micro-CT finite element models of mouse bone. Proceedings of the 58th Annual Meeting of the Orthopaedic Research Society, 2011

6. **Bhatia V.A.**, Edwards W.B., Troy K.L.: Repeatability of image registration and segmentation procedures for CT scans of the human distal radius? Proceedings of the 36th Annual Meeting of the American Society of Biomechanics, 2012

7. Troy K.L., **Bhatia V.A.**, Edwards W.B.: Compressive loading of the distal radius improves bone structure in young women? Proceedings of the 36th Annual Meeting of the American Society of Biomechanics, 2012

8. **Bhatia V.A.**, Edwards W.B., Troy K.L.: Predicting bone adaptation at the human distal radius using cadaveric specimens and the Daily Strain Stimulus theory. Proceedings of the 59th Annual Meeting of the Orthopaedic Research Society, 2013

9. **Bhatia V.A.**, Edwards W.B., Troy K.L.: Finite element prediction of periosteal strain at the human distal radius during a targeted loading task. Proceedings of the 37th Annual Meeting of the American Society of Biomechanics, 2013